INFORMATION TO USERS

This manuscript has been reproduced from the microfilm master. UMI films the text directly from the original or copy submitted. Thus, some thesis and dissertation copies are in typewriter face, while others may be from any type of computer printer.

The quality of this reproduction is dependent upon the quality of the copy submitted. Broken or indistinct print, colored or poor quality illustrations and photographs, print bleedthrough, substandard margins, and improper alignment can adversely affect reproduction.

In the unlikely event that the author did not send UMI a complete manuscript and there are missing pages, these will be noted. Also, if unauthorized copyright material had to be removed, a note will indicate the deletion.

Oversize materials (e.g., maps, drawings, charts) are reproduced by sectioning the original, beginning at the upper left-hand corner and continuing from left to right in equal sections with small overlaps. Each original is also photographed in one exposure and is included in reduced form at the back of the book.

Photographs included in the original manuscript have been reproduced xerographically in this copy. Higher quality 6" x 9" black and white photographic prints are available for any photographs or illustrations appearing in this copy for an additional charge. Contact UMI directly to order.

UMI

A Bell & Howell Information Company
300 North Zeeb Road, Ann Arbor MI 48106-1346 USA
313/761-4700 800/521-0600

STATISTICS OF MICROWAVE RADIATION IN THE APPROACH TO LOCALIZATION

by

MARIN STOYTCHEV

A dissertation submitted to the Graduate Faculty in Physics in partial fulfillment of the requirements for the degree of Doctor of Philosophy, The City University of New York.

1998

This manuscript has been read and accepted for the Graduate Faculty in Physics in satisfaction of the dissertation requirement for the degree of Doctor of Philosophy.

4/23/98
Date

Chair of Examining Committee

4/28/98
Date

Executive Officer

Joel I. Gersten, City College

Alexander Lisyansky, Queens College

Harold Metcalf, SUNY Stony Brook

Steven A. Schwarz, Queens College

Supervisory Committee

THE CITY UNIVERSITY OF NEW YORK

To Narciso Garcia,

a teacher and a friend whom I dearly miss.

Acknowledgments

I wish to thank my supervisor Dr. Azriel Genack for the generous help and his guidance throughout this work. His expertise has been crucial for the successful completion of this research. I am grateful to Dr. Narciso Garcia for being always there for me when I needed support and encouragement the most. I would like to thank Dr. Alexander Lisyansky for the valuable help at some stages of this work. I would like to thank Dr. Michael Kempe, Dr. Dmitry Livdan, Mr. Andrey Chabanov, and Mr. Victor Podolsky for the fruitful discussions and friendly advice. I would like to thank Mr. Walter Polkosnik and Mr. Dmitry Zaslavsky for helping me learn enough about computers and computing so that I managed to accomplish this part of the work on acceptable level. I would like to thank Mr. Grigory German. Mr. Ed Kuhner, and Mr. Ziggy Ozimkovski for their expert technical assistance.

I would like to thank Dr. Joel Gersten, Dr. Harold Metcalf, Dr. Steven Schwartz. and Dr. Alexander Lisyansky for being kind to serve in my thesis Supervisory Committee.

I thank my wife Nora and my son Stoytcho for bearing with me during the many years of study.

It is my pleasure to extend my gratitude to all members of the Faculty and Staff at the Department of Physics at Queens College.

Finally, I would like to acknowledge the contribution, in the form of discussions or communications of results and ideas, of Dr. Mark van Rossum, Dr. Piet Brouwer,

Dr. Eugene Kogan, Dr. Boris Shapiro, Dr. Reuven Pnini, Dr. Patrick Sebbah, Dr. Bart van Tiggelen, Dr. Costas Soukoulis, and Dr. Michalis Sigalas.

This work is part of the ongoing research on wave propagation in random media which is supported by the National Science Foundation and by PSC-CUNY.

Contents

List of Figures

1 Introduction

The propagation of classical wave through random media affects many aspects of everyday life. Information carried by sound, light, radio and microwave radiation is transmitted through media which, in general, vary randomly in time and space so that the amplitude and the phase of the waves fluctuate randomly in time and space. [1] Extracting information from this "random" signal and investigating the origin of these fluctuations has been of interest through the ages. [2,3] In this thesis we study steady state transport in multiply scattering media consisting of randomly positioned scatterers. Interference between scattered waves leads to large fluctuations in key transmission quantities - intensity, total transmission, and total transmittance, which corresponds to the dimensionless conductance g. Because of the pervasiveness of fluctuations, a full description of transport must provide not only the averages but the variances and the full distributions of these transmission quantities. [4]

Interest in the problem has intensified with the recognition of the analogy between classical and quantum waves in disordered systems. In the mid-eighties fluctuations of the electronic conductance of order of unity were observed in disordered conductors cooled below 1 K. [5,6] These fluctuations appeared to be independent of sample parameters such as the conductance itself, the size of the sample or the transport mean free path ℓ of the electrons in the sample and were therefore named universal conductance fluctuations (UCF). Such fluctuations were explained by consid-

ering the interference processes between electron waves. [7,8] The discovery of UCF and the predictions and the observations of coherent backscattering [9,10], short- [11–14] and long-range [15–25] intensity correlation, photon localization [26–32], and the photonic band gap [33] have been of particular importance for the development of a new field now known as Mesoscopic Physics. It deals with transport in random systems in which the waves are temporally coherent throughout the sample.

In 1958, Anderson proposed that electrons could become localized by a randomly varying potential. [34] In multiple-scattering media, the interference processes may become so strong that normal diffusion vanishes with the dimensionless conductance g becoming smaller than unity. Following the analogy between electrons and classical waves in mesoscopic systems, the possibility of localizing classical waves in strongly scattering media was suggested. [26–30] In a proof of principle experiment of microwave transmission in a three dimensional (3D) periodic metal wire network. it was shown that classical wave localization due to strong scattering is possible [35]. Recently, localization of infrared light in strongly scattering samples of pure GaAs particles was observed by Wiersma et. all. [36] Localization due to strong scattering was achieved also in microwave experiments in quasi-1D samples of alumina spheres by Chabanov and Genack [37].

Strong intrinsic scattering can be evaluated in terms of the product of the wave number k and the transport mean three path ℓ of the wave in the system. The condition for localization due to strong scattering is given by the Ioffe-Riegel criterion $k\ell \leq 1$ [38], which implies that the wave scatters in a distance of order or

smaller than the wavelength. This strong condition must be met in the case of a unbounded 3D system, but is not necessary for samples on which spatial boundaries are imposed.

It was first suggested by Thouless that electrons will always be localized in sufficiently long wires at low temperatures. [39] This approach to localization can be viewed as a particular realization of the localization condition $g \leq 1$. In connection with this, we note that the dimensionless conductance, which is a central parameter in the description of the statistics of mesoscopic transport [40], can be used in a different context in the description of wave transport. Here, we consider three ways in which the dimensionless conductance is a central parameter in the description of the statistical properties of transmission quantities. The definition of the conductance of a particular system comes from the scattering theory approach pioneered by Landauer [41]. According to this approach, the conductance equals the total transmission when all input modes are present. In this case, the average value of the conductance g is given as $g = N\ell/L$, where N is the total number of input modes, L is the sample length, and ℓ is the transport mean free path. The average value of total transmission for one input mode is ℓ/L. The localization threshold is reached at $g = 1$ which determines the localization length of the sample $\xi = N\ell$. For $L > \xi$, the transmission through the sample decreases exponentially with increasing L. [40] Another way to describe the transition to localization is provided by considering the conductance of the system as the ratio between the level width δE of energy states (modes) and the level spacing ΔE, $g \equiv \delta = \delta E/\Delta E$ (δ is known

as the Thouless number) [42]. When this ratio is much greater than unity, different modes (states of the system) overlap creating a conductance band and the system is in metallic regime. If, however, the Thouless number is smaller than one, the modes are localized and the sample is an insulator. The localization condition is again given by $g = 1$. Finally, in the probabilistic world, the reciprocal value of the conductance $1/g$ gives the probability for a wave to return to a coherent volume. The first two aspects are associated with finite systems and reflect boundary conditions and indicate that localization can be achieved when $g \sim 1$ even when $k\ell > 1$. The criterion $k\ell \leq 1$ is analogous to the condition for localization associated with the probabilistic meaning of g in the case of a 3D system. It is important, however, not only to achieve classical wave localization , but also to give a full statistical description of wave transport in this process.

In this thesis, we investigate the changing character of the statistics of wave transport in the approach to the localization and provide a quantitative description of the distributions of intensity and total transmission of microwave radiation near the localization threshold.

The thesis is organized as follows. In **chapter 2**, we give an overview of wave transport in mesoscopic systems. The key transmission quantities are presented using the scattering theory approach of Landauer. [41] The different terms contributing to the intensity correlation function, which determine the magnitude of fluctuations in transmission quantities are discussed. In this chapter, we describe briefly the two theoretical approaches - diagrammatic field theory and random ma-

trix theory (RMT) - the results of which are heavily used in the analysis of the measured distributions of intensity and total transmission. The diagrammatic approach uses an expansion in the small parameter $1/g$ and is expected to provide an adequate description of wave transport only in the diffusive regime of propagation ($g \gg 1$). It appears, however, that this approach, when modified appropriately, can describe fluctuations in samples with small values of g as well. [43] RMT does not require the condition $g \gg 1$ and is particularly useful for studying the transition to localization. This approach, however, uses the isotropic approximation which assumes perfect mixing of modes. [44] It can be used in describing wave transport in quasi-1D samples in which the sample length is much greater than its cross-sectional diameter d. At the end of chapter 2 we discuss the possibilities and the difficulties which exist in microwave experiments.

In **chapter 3**, we study the statistics of total transmission in quasi-1D random samples with small values of the dimensionless conductance. Recently, an expression for the probability distribution of total transmission in terms of g for non-absorbing samples was obtained by Nieuwenhuizen and van Rossum using diagrammatic techniques combined with RMT [45] and subsequently by Kogan and Kaveh using the RMT approach [46]. The distribution was proposed to be Gaussian with a non-Gaussian tail. In optical experiments with samples with $g \sim 10^3$, de Boer et. al observed small but clear deviations from Gaussian distribution. [47] In microwave measurements in samples with small values of g ($g \lesssim 10$), we observe distinctively non-Gaussian distributions. [43] Surprisingly, we find that the measured transmis-

sion distributions are adequately described by the theory [45,46] when the measured variance of the distribution, which equals the degree of nonlocal intensity correlation, is used as a characteristic parameter in the theoretical expression. The variance of the total transmission distribution normalized to its ensemble average value, however, is found to increase sublinearly with sample length. This is in contrast to the superlinear increase expected from the theory in the absence of absorption. This result is associated, therefore, with the affect of absorption on the statistics of wave transport and raises the question of whether localization can be achieved in strongly absorbing samples.

In **chapter 4**, we present measurements of intensity distributions for the same samples as those used in the measurements of total transmission. Here, however, measurements were made for sample lengths as large as the localization length ξ (more than twice as large as the maximum length used in the measurements of total transmission). [48] These measurements allows us to investigate fundamental issues of the statistics of mesoscopic transport. Recently, Kogan and Kaveh proposed a relationship between the moments of intensity and total transmission. Using this relation, the intensity distribution can be obtained as a transform of the total transmission distribution. [46] We confirm experimentally the relationship between the moments of these transmission quantities and the relationship between the corresponding distributions. This allows us to investigate the scaling of the variance of total transmission using measurements of the intensity distributions for lengths up to the localization length. We find that the variance of the normalized transmission

increases superlinearly with length near the localization length even in the presence of strong absorption. This result indicates that absorption does not destroy localization. We also demonstrate that field measurements provide means for statistically eliminating the influence of absorption on wave transport. This facilitates the determination of ξ and allows us to clarify the interplay between absorption and localization. Our results, show that the variances of intensity and total transmission are reliable measures of the closeness to the localization threshold.

In **chapter 5**, we obtain the absorption length and the diffusion constant of the samples discussed in chapters 3 and 4 from the field autocorrelation function with frequency shift. We show also that the variance of the total transmission equals the degree of nonlocal intensity correlation across the output face of the sample. Finally, we present measurements of the long- ($C2$) and infinite-range (C_3) terms of the intensity correlation function with frequency shift.

In **chapter 6**, an alternative approach to localization - photonic band gap (PBG) materials - is discussed. In this approach, localization can be achieved by tuning the frequency of the radiation through the edge of the photonic band gap, in contrast to the approach employed in chapters 3 and 4 in which the sample dimensions were changed in order to achieve localization. The possibility of creating periodic dielectric structures which possess a photonic band gap (PBG) was first discussed by E. Yablonovitch [33] and S. John [49] in 1987. Since then, the band structure for various 3D dielectric [50–53] and metallic [54–56] periodic structures possessing band gaps have been calculated and dielectric [50,57–59] and metallic [60] systems

possessing band gaps have been constructed. If disorder is introduced into a PBG material it is possible to create a localized state within the band gap which has been demonstrated in many works. [50] The statistics of localization have not been explored, however, for states associated with defects. In a proof of principal experiment, we use a 3D cubic metal structure possessing photonic band gap and show that the statistics of the localization transition can be studied for an ensemble of strong scatterers randomly positioned inside the photonic crystal. [35]

We conclude the thesis with a **summary** of the main results of this work.

2 Wave Transport in Mesoscopic Systems

2.1 Key transmission quantities - their averages, fluctuations and correlations

The term mesoscopic systems has its origin from the submicron size of the disordered conductors in which below 1 K UCF have been observed [5,6]. The submicron dimensions of the samples (in the case of electronic transport) are in the intermediate regime between the atomic (microscopic) scale and the everyday macroscopic scale, hence the name "mesoscopic". Mesoscopic systems are sufficiently small that electrons (or waves) maintain their phase coherence, so that the classical description of transport is inadequate. On the other hand, they are sufficiently large that a statistical description is meaningful. In order to maintain phase coherence, the sample must be smaller than the characteristic phase coherence length L_φ determined by the strength of inelastic scattering.

The statistical behavior of electron transport encountered in mesoscopic samples is only quantum mechanical in that it derives from the wavelike behavior of electrons and analogous statistical behavior is present in any system in which waves propagate by multiple coherent scattering. The analogy between quantum and classical wave transport emerges clearly from the scattering theory approach pioneered by Landauer [41]. In this approach, the electronic conductance can be expressed solely in terms of the transmission coefficients of the sample considered as a single, com-

plex scattering center. Here we present briefly the arguments leading to the simplest expression of this type as they appeared in the work of Stone et. al on random matrix theory and maximum entropy models in disordered conductors [61]. An ideal two-probe measurement is considered in which the sample is attached between two perfect reservoirs with electrochemical potentials μ_1 and $\mu_2 = \mu_1 + eV$, respectively, where V is the applied voltage. These reservoirs serve both as current source and sink and as voltage terminals. The total current which flows through the sample can be obtained from a "counting argument". In the energy interval eV between μ_2 and μ_1 electrons are injected into right-going states emerging from reservoir 1, but none are injected into left-going states emerging from reservoir 2. Thus there is a net right-going current proportional to the number of states in the interval $\mu_1 - \mu_2$, given by

$$I = e\sum_{i}^{N} v_i \frac{dn_i}{d\varepsilon} eV \sum_{j}^{N} T_{ij} = \left[(e^2/h) \sum_{i,j}^{N} T_{ij} \right] V = (e^2/h) g V, \qquad (1)$$

where N is the number of propagating channels in the sample, v_i is the longitudinal velocity for the ith momentum channel at the Fermi surface, T_{ij} is the transmission probability from i to j, and g is the dimensionless conductance. For a quasi-1D system the density of states is $dn_i/d\varepsilon = 1/hv_i$. *

---

*In the description of classical wave transport, the letters a and b are used as subindexes to indicate different modes instead of the letters i and j as given in Eq. (1). The "classical wave" notation will be used throughout the rest of this thesis.

This approach can be directly applied to classical wave transport in random media. The key transmission quantities in order of increasing spatial averaging are the intensity, T_{ab}, which is the transmission coefficient for incoming mode a into mode b, the total transmission for incoming mode a, $T_a = \sum_b T_{ab}$, and the total transmittance $T = \sum_{ab} T_{ab}$. The total transmittance is equivalent to the dimensionless conductance in electronic systems, $T = g$. Schematic presentation of these quantities is given in Fig. 1.

In describing wave transport in random media, there are important characteristic lengths which define the regime of propagation. A mean free path is a characteristic length scale which is generally introduced to describe the scattering process. In multiple scattering processes, the system is characterized by the transport mean free path ℓ, which is the average distance in which the direction of propagation of the wave is randomized. If the sample length L is much larger than the transport mean free path, $L \gg \ell$, and away from the localization threshold, $g \equiv \xi/L \gg 1$. wave transport is described by diffusion theory. The diffusive regime is then given by $\ell \ll L \ll \xi$. When L becomes comparable to ξ, localization corrections must be taken into account.

Another length scale of particular importance is the absorption length L_a which is defined as the traveled length over which the intensity is reduced by a factor of $1/e$ due to loses in the medium. In the diffusive regime of propagation $L_a = (D\tau_a)^{1/2}$, where $1/\tau_a$ is the absorption rate and D is the diffusion coefficient. Absorption is often neglected in theoretical models. In reality, however, absorption is generally of

importance to an extent determined by the ratio L/L_a. Systems then can be considered as weakly absorbing ($L < L_a$) or strongly absorbing ($L \gg L$). In the later case the influence of absorption upon the behavior of certain transport parameters could be significant. This is for example the case of the average values of the transmission quantities which fall exponentially with sample length due to the presence of absorption. Because localization also leads to an exponential decay of transmission it can be difficult to disentangle the influence of absorption and localization on transmission. In this work, we find, however, that absorption affects only marginally the statistics of intensity and total transmission and the variances of these quantities serve as reliable measures to the closeness to the localization threshold.

In the diffusive regime the statistical averages of intensity, total transmission, and transmittance are given by $<T_{ab}>= \ell/NL$, $<T_a>= \ell/L$, and $<T>= g = N\ell/L$. Because of wave interference these transmission quantities exhibit significant fluctuations from their ensemble average values. Typical spectra of intensity and total transmission normalized by their ensemble averages, $s_{ab} = T_{ab}/ <T_{ab}>$ and $s_a = T_a/ <T_a>$, measured in samples with $g \approx 10$ are shown in Fig. 2.

The intensity is the least spatially averaged quantity and exhibits the largest fluctuations. Even for $g \gg 1$, its variance equals one, whereas the variance of total transmission is of order of $1/g$. We note also the difference between the width of the peaks observed in the intensity spectrum and that in the case of total transmission. This illustrates the well known fact that the with of the intensity correlation function with frequency shift is determined by the short-range correlation (C_1 term)

and is much smaller than the correlation frequency in total transmission which is determined by long-range correlation (C_2 term). In Fig. 3, we show total transmission spectra for two different sample configurations which illustrate the large sample to sample fluctuations of the transmittance quantities. On the contrary, the spectrum for a given sample configuration is highly reproducible. This can be seen from the difference between the two spectra taken for the same sample configuration which is shown in the bottom part of the figure. Similar fluctuations are observed when one moves the detector across the output face of the sample while keeping the frequency of the radiation fixed. A typical example of spatial fluctuations is the spectrum observed when the laser beam is transmitted through a slab containing random scatterers.

The magnitude of the spectral and spatial fluctuations in the transmission quantities is determined by the spectral and spatial correlation of intensity inside the sample. In a waveguide geometry in which modes are perfectly mixed, the ensemble average of T_{ab}, $<T_{ab}>$, does not depend on a or b. The correlation matrix, $C_{aba'b'} = <\delta T_{ab}\delta T_{a'b'}> \; / \; <T_{ab}>$ ($\delta T_{ab} \equiv T_{ab} - <T_{ab}>$), is then the sum of three distinct terms, [17,19,62]

$$C = C_1 + C_2 + C_3 = A_1\delta_{aa'}\delta_{bb'} + A_2(\delta_{aa'} + \delta_{bb'}) + A_3, \qquad (2)$$

where, to second order in the small parameter $1/g$, the coefficients A_1, A_2, and A_3 are given by $A_1 = \gamma(1+\frac{2}{15g^2})$, $A_2 = \gamma(\frac{2}{3g}+\frac{2}{15g^2})$, $A_3 = \gamma\frac{2}{15g^2}$ with $\gamma = (1-\frac{1}{3g}+\frac{1}{45g^2})^{-1}$. [63] The first term describes shot-range correlation and dominates fluctuations of

T_{ab}. The second term describes long- range correlation and determines fluctuations of T_a. The last term represents infinite-range correlation and dominates the fluctuations in T. It is the degree of nonlocal correlation (C_2+C_3) which is the source of the deviations of intensity from negative exponential statistics and of total transmission from a normal distribution which have been predicted [45,46,64] and experimentally observed [22,43,47,65] in studies of the statistic of wave transport in random media. As the extent of spatial averaging increases, the variances of the normalized transmission quantities , s_{ab}, s_a and $s(= T/<T>)$, are reduced. However, these quantities do not self average, as they would if spatial correlation were absent. To leading order in $1/g$, the variances of s_{ab}, s_a, and s arising from nonlocal correlation for diffusing waves are 1, $2/3g$, and $2/15g^2$ [17,19] corresponding to enhancement of 1, L/ℓ [16], and $(L/\ell)^2$ [7,8], respectively.

2.2 Theoretical approaches

In this section, we briefly introduce two theoretical approaches, the results of which are used in the analysis of the measured intensity and transmission distributions presented here, namely the diagrammatic approach and the RMT approach.[†]

In considering the diagrammatic Green's function approach we will treat the stationary field $\mathbf{E}(\mathbf{r})$. The electric field satisfies the time-independent Helmholtz equation

$$\nabla^2 E(\mathbf{r}) + \frac{\omega^2}{c^2}\epsilon(\mathbf{r})E(\mathbf{r}) = 0, \tag{3}$$

where $E(\mathbf{r})$ denotes one of the field's components, $\epsilon(\mathbf{r})$ is the (spatially random) dielectric constant of the system, ω is the frequency, and c is the speed of light in vacuum. The wave equation can be rewritten as

$$\nabla^2 E(\mathbf{r}) + \frac{\omega^2}{c^2}E(\mathbf{r}) = V(\mathbf{r})E(\mathbf{r}), \tag{4}$$

where $V(\mathbf{r})$ is the scattering potential defined as $V(\mathbf{r}) \equiv -(\omega/c)^2[\epsilon(\mathbf{r}) - 1]$. For a

---

[†]The reader should not expect to see here development of these approaches in order to solve particular problems and the solutions of such. Great deal of work has been done on wave propagation in random media (mesoscopic systems) using both approaches. The author of this thesis is most familiar with the work of Th. M. Nieuwenhuizen and M. C. W. van Rossum on Green's functions diagrammatic approach (see Ph. D. thesis of M. C. W. van Rossum [66] and references therein) and the work of C. W. J. Beenakker and co-authors on RMT approach (for an updated review on RMT see Ref. [67]).

collection of point-like scatterers with polarizability α_0 in a surrounding medium with dielectric constant of unity, the scattering potential is given by

$$V(\mathbf{r}) = -\frac{\alpha_0 \omega^2}{c^2} \sum_i \delta(\mathbf{r} - \mathbf{r}_i), \tag{5}$$

with $\mathbf{r}_i$ denoting the position of the scatterers.

Introducing the Green's function $G_0(\mathbf{r}_1, \mathbf{r}_2)$ as the solution of the equation

$$\nabla^2 G_0(\mathbf{r}_1, \mathbf{r}_2) + \frac{\omega^2}{c^2} G_0(\mathbf{r}_1, \mathbf{r}_2) = -\delta(\mathbf{r}_1 - \mathbf{r}_2), \tag{6}$$

one can write the solution for the field in Eq. (4) formally as

$$E(\mathbf{r}_1) = E_{in}(\mathbf{r}_1) - \int d\mathbf{r}_2 G_0(\mathbf{r}_1, \mathbf{r}_2) V(\mathbf{r}_2) E(\mathbf{r}_2), \tag{7}$$

where $E_{in}(\mathbf{r}_1)$ represents the incoming coherent wave. $G_0(\mathbf{r}_1, \mathbf{r}_2)$ is also referred to as a bare Green's function and describes propagation of the field in a medium without scatterers. It is given by

$$G_0(\mathbf{r}_1, \mathbf{r}_2) = \frac{exp(-ik \mid \mathbf{r}_1 - \mathbf{r}_2 \mid)}{4\pi \mid \mathbf{r}_1 - \mathbf{r}_2 \mid}, \tag{8}$$

where $k = \omega/c$ is the wave number.

To describe the propagation of the field in the medium independent of E_{in}, we use the total Green's function $G(\mathbf{r}_1, \mathbf{r}_2)$ which is defined as a solution of

$$\nabla^2 G(\mathbf{r}_1, \mathbf{r}_2) + \frac{\omega^2}{c^2} \epsilon(\mathbf{r}) G(\mathbf{r}_1, \mathbf{r}_2) = -\delta(\mathbf{r}_1 - \mathbf{r}_2), \tag{9}$$

The Green's function $G(\mathbf{r}_1, \mathbf{r}_2)$ describes the field at any point $\mathbf{r}_1$ in the medium, due to a source at $\mathbf{r}_2$. It can be presented as perturbation series as

$$G(\mathbf{r_1},\mathbf{r_2}) = G_0(\mathbf{r_1},\mathbf{r_2}) - \int d\mathbf{r_a} G_0(\mathbf{r_1},\mathbf{r_a}) V(\mathbf{r_a}) G_0(\mathbf{r_a},\mathbf{r_2}) \qquad (10)$$

$$+ \int\int d\mathbf{r_a} d\mathbf{r_b} G_0(\mathbf{r_1},\mathbf{r_a}) V(\mathbf{r_a}) G_0(\mathbf{r_a},\mathbf{r_b}) V(\mathbf{r_b}) G_0(\mathbf{r_b},\mathbf{r_2}) - \cdots .$$

The first term of Eq. (10) describes propagation without scattering, the second term equals the sum of all single scattering contributions, the third term - the sum of all double scattering contributions, etc. To simplify the notation, Feynman diagrams are used. The diagrammatic representation of the above series is shown in Fig. 4a. The lines represent the bare Green's function $G_0(\mathbf{r_1},\mathbf{r_2})$ and the circles represent the scattering potential of an individual scatterer, $-\alpha_0(\omega/c)^2\delta(\mathbf{r_1}-\mathbf{r_2})$. Dashed lines connect identical scatterers. The above series can be further simplified by introducing the single particle t-matrix $t(\mathbf{r_1},\mathbf{r_2},\omega)$ (diagrammatic representation: $\times$) defined as the sum of all repeated scattering events from one scatterer (Fig. 4b). The resulting diagrammatic presentation of the total Green's function using the t-matrix of a single scatterer is shown in Fig. 4c. The perturbation series for the t-matrix is called the Born series. The physical interpretation of this series is that the incoming field induces an electric polarization (first term). This polarization changes the field around the scatterer, and this change in turn affects the polarization again (second term), etc. The t-matrix of a point scatterer located at $\mathbf{r_i}$ is to first order $t(\mathbf{r_1},\mathbf{r_2},\omega) = \alpha_0(w/c)^2\delta(\mathbf{r_2}-\mathbf{r_i})\delta(\mathbf{r_1}-\mathbf{r_i})$.

If one considers the field and takes average over the positions of the scatterers to obtain statistical parameters, all interference processes are lost. In order to account for wave interference the intensity of the field must be considered. In terms of the

total Green's function, the intensity is given by

$$I(\mathbf{r}) \equiv E(\mathbf{r})E^*(\mathbf{r}) = \int\int d\mathbf{r_1}d\mathbf{r_2}G(\mathbf{r},\mathbf{r_1})G^*(\mathbf{r},\mathbf{r_2})E_{in}(\mathbf{r_1})E^*_{in}(\mathbf{r_2}). \qquad (11)$$

The product GG^* defines the intensity propagator $R(r_1, r_2; r_3, r_4) \equiv G(r_1, r_2) \times G(r_3, r_4)$ which describes the intensity at any point in the system due to the product of the incoming waves $E_{in}E^*_{in}$. The diagrammatic expansion of R is presented in Fig. 5a. The upper line corresponds to $G(\mathbf{r_1}, \mathbf{r_2})$ and the lower line to the complex conjugate $G^*(\mathbf{r_1}, \mathbf{r_2})$. Dashed lines again connect identical scatterers. The statistical properties of transport then are given by the ensemble average $<R(r_1, r_2; r_3, r_4)>$, where angular brackets denote averaging over disorder. The goal of this approach is to obtain $<R(r_1, r_2; r_3, r_4)>$. To lowest order in scatterers density, the intensity propagator can be approximated as built up of the so called "ladder" diagrams (Fig. 5b). Higher order corrections are included when various terms of the "most crossed" diagrams are taken into account some of which are shown in Fig. 5c.

While the diagrammatic approach attempts to build the scattering matrix of the system as a whole from the scattering matrix of an individual scatterer, RMT considers the whole system as a single scatterer. In our presentation we follow a recent work by Beenakker [67]. Although, this work deals specifically with quantum transport in mesoscopic conductors it provides an updated overview of mesoscopic wave transport in general.

A mesoscopic conductor is modeled by an elastically scattering disordered region connected by ideal leads (without disorder) to two electron reservoirs (see Fig. 6).

All inelastic scattering is assumed to take place in the reservoirs, which are in equilibrium at zero temperature. The ideal leads are "electron waveguides", introduced to define a basis for the scattering matrix of the disordered region.

The wave function $\Psi(\mathbf{r})$ of an electron in a lead at energy E_F separates into a longitudinal and a transverse part, $\Psi_n^{\pm}(\mathbf{r}) = \Phi_n(y,z)exp(\pm ik_n x)$. The integer $n = 1, 2, ..., N$ labels the propagating modes, also referred to as scattering channels. Mode n has a real wave number $k_n > 0$ and transverse wave function Φ_n. (For simplicity of notation, the two leads are assumed to be identical.) The normalization of the wave function Ψ is chosen such that it carries unit current. A wave incident on the disordered region is thus described by a vector of coefficients $c^{in} \equiv (a_1^+, a_2^+, ..., a_N^+, b_1^-, b_2^-, ..., b_N^-)$ describing the amplitudes of the incident modes. The first set of N coefficients refers to the left lead and the second set of coefficients to the right lead as shown in Fig. 6. Similarly, the reflected and transmitted wave is a vector with coefficients $c^{out} \equiv (a_1^-, a_2^-, ..., a_N^-, b_1^+, b_2^+, ..., b_N^+)$. The scattering matrix S is a $2N \times 2N$ matrix which relates these two vectors,

$$c^{out} = \mathbf{S}c^{in}. \tag{12}$$

It has the block structure

$$\mathbf{S} = \begin{pmatrix} \mathbf{r} & \mathbf{t}' \\ \mathbf{t} & \mathbf{r}' \end{pmatrix}, \tag{13}$$

with $N \times N$ reflection matrices $\mathbf{r}$ and $\mathbf{r}'$ (reflection from left to left and from right to right) and transmission matrices $\mathbf{t}$ and $\mathbf{t}'$ (transmission from left to right and from

right to left).

Current conservation requires that $\mathbf{S}$ is a unitary matrix: $\mathbf{S}^{-1} = \mathbf{S}^{\dagger}$. It is a consequence of unitarity that the four Hermitian matrices $\mathbf{t}\mathbf{t}^{\dagger}$, $\mathbf{t}'\mathbf{t}'^{\dagger}$, $1 - \mathbf{r}\mathbf{r}^{\dagger}$, and $1 - \mathbf{r}'\mathbf{r}'^{\dagger}$ have the same set of eigenvalues $T_1, T_2, ..., T_N$. Each of these N transmission eigenvalues is a real number between 0 and 1. The scattering matrix can be written in terms of T_n's by mean of the polar decomposition [17,68]

$$\mathbf{S} = \begin{pmatrix} \mathbf{U} & \mathbf{0} \\ \mathbf{0} & \mathbf{V} \end{pmatrix} \begin{pmatrix} -\sqrt{1-\mathcal{T}} & \sqrt{\mathcal{T}} \\ \sqrt{\mathcal{T}} & \sqrt{1-\mathcal{T}} \end{pmatrix} \begin{pmatrix} \mathbf{U}' & \mathbf{0} \\ \mathbf{0} & \mathbf{V}' \end{pmatrix}. \tag{14}$$

Here U, V, U', V' are four $N \times N$ unitary matrices and $\mathcal{T}$ is a $N \times N$ diagonal matrix with the transmission eigenvalues on the diagonal. ‡

The *scattering matrix* relates incoming to outgoing states. The *transfer matrix* relates states in the left lead to states in the right lead. A wave in the left lead can be represented by a vector $c^{left} \equiv (a_1^+, a_2^+, ..., a_N^+, a_1^-, a_2^-, ..., a_N^-)$ with the first set of N coefficients referring to incoming waves and the second set of coefficients to outgoing waves. Similarly, a wave in the right lead can be represented by a vector $c^{in} \equiv (b_1^+, b_2^+, ..., b_N^+, b_1^-, b_2^-, ..., b_N^-)$. The transfer matrix $\mathbf{M}$ is a $2N \times 2N$ matrix that relates these two vectors,

$$c^{right} = \mathbf{M} c^{left}. \tag{15}$$

---

‡For the constraints imposed on the scattering matrix depending on the symmetry present see the work by Beenakker [67]

The scattering and transfer matrices are equivalent descriptions of scattering from the disordered region. A convenient property of the transfer matrix is the *multiplicative* composition rule - the transfer matrix of a number of disordered regions in series (separated by ideal leads) is the product of the individual transfer matrices. Thus, the transfer matrix can be readily used to investigate the scaling of mesoscopic transport. The scattering matrix, in contrast, has a more complicated composition rule (involving matrix inversion) and cannot be directly used in a scaling approach. By expressing the elements of $\mathbf{M}$ in terms of the elements of $\mathbf{S}$ one obtains the polar decomposition of the transfer matrix [17],

$$\mathbf{M} = \begin{pmatrix} \mathbf{V} & \mathbf{0} \\ \mathbf{0} & \mathbf{V}'^{\dagger} \end{pmatrix} \begin{pmatrix} \sqrt{T^{-1}} & \sqrt{T^{-1}-1} \\ \sqrt{T^{-1}-1} & \sqrt{T^{-1}} \end{pmatrix} \begin{pmatrix} \mathbf{U}' & \mathbf{0} \\ \mathbf{0} & \mathbf{U}^{\dagger} \end{pmatrix}, \tag{16}$$

in terms of the same $N \times N$ matrices used in Eq. (14).

The transmission eigenvalues determine a variety of transport properties. First of all is the conductance $G = \lim_{V \to 0} \bar{I}/V$, defined as the ratio of the time-averaged electrical current $\bar{I}$ through the conductor and the voltage difference V between the two electron reservoirs in the limit of vanishingly small voltage. At zero temperature, the conductance is given by

$$G = G_0 \sum_{j}^{N} T_n, G_0 \equiv \frac{2e^2}{h}. \tag{17}$$

The factor of two in G_0 accounts for the twofold spin degeneracy.

As an illustration of the description of wave transport in terms of transmission eigenvalues we give the explanation of UCF made by Imry [69]. Imry's argument con-

trasts "closed" and "open" scattering channels. Most transmission eigenvalues in a disordered conductor are exponentially small. These are the closed channels. A fraction ℓ/L of the total number N of transmission eigenvalues is of order of unity. These are the open channels. Only the open channels contribute effectively to the conductance giving a value of the dimensionless conductance $g = G/G_0 \equiv N_{eff} \approx N\ell/L$. Fluctuations in the conductance can be interpreted as fluctuations in the number N_{eff} of open channels. The picture of "closed" and "open" channels of propagation is described mathematically by the bimodal (Dorokhov [70]) distribution of the transmission eigenvalues $\rho(\tau)$ which is shown in Fig. 7 in the case of nonabsorbing systems. The distribution $\rho(\tau)$ has been used to calculate the probability distribution of total transmission [45,46,73,79]. Consequently, the relationship between the statistics of intensity and total transmission is used in order to obtain the probability distribution of intensity. [46]

To summarize, RMT of mesoscopic transport addresses the following two questions. What is the ensemble of scattering matrices for a particular system? How does one obtain the statistics of transport properties from this ensemble?

2.3 Microwave experiments - possibilities and difficulties

In classical wave experiments it is possible in principle to measure all three transmission quantities. In optical experiments one measures readily intensity in the far field and total transmission. In microwave experiments one usually measures the near field. Measurements of conductance, however, in classical wave experiments have not been reported yet. In contrast, one directly measures the conductance in studies of electronic transport. In studies of the statistics of wave transport, the ability to create an ensemble of statistically equivalent sample configurations is of particular importance. An ensemble of statistically equivalent sample configurations can be easily realized in the case of classical waves by physically changing the position of the scatterers inside the sample. In the case of electrons one does not have an ensemble of different sample configurations. Instead, a varying magnetic field is used to simulate different sample configurations. In this case, however, the time reversal symmetry of the system is broken. This can lead to some differences in the statistics of transport as compared to systems in which time reversal symmetry is preserved.

Microwave experiments are practically well suited for studying fundamental issues of the statistics of wave transport in random media among experiments in which classical waves are used (light in particular). Because of the relatively large wavelength of the radiation, $\lambda \sim 1$ cm, appropriate samples can be easily realized. Here, one can readily achieve different regimes of propagation either by changing the properties of the individual scatterers or by varying the macroscopic dimensions

of the system - its length and/or cross-sectional area for example. The large size of scatterers makes it possible to produce a statistical ensemble of random sample configurations. Using microwave radiation one can measure both the amplitude and the phase of the field transmitted through the sample. Thus, such measurements provide the complete information necessary to describe wave transport. This makes it possible to investigate different aspects of the statistics of transport in mesoscopic systems in different regimes of propagation including ballistic, diffusive, critical, and localized regimes. Also, very accurate measurements can be carried out so that adequate comparison with theoretical prediction can be made. In this thesis, we report studies of the statistics of wave transport in the approach to localization using microwave radiation. Small values of the dimensionless conductance are achieved by increasing the length of samples with quasi-1D geometry and by tuning the frequency of radiation through the edge of the band gap of a "photonic crystal" in which localized states are created by introducing disorder.

Among the realities that microwaves experiments encounters the presence of absorption is probably the most significant. A trivial problem arising from the presence of absorption is the attenuation of the transmitted signal, thus making difficult measurements with low level signals. Another problem which concerns wave localization is the fact that both absorption and localization give rise to exponential decay of transmission which makes difficult to distinguish localization from absorption affects on transmission in strongly absorbing samples. It is therefore important that the influence of absorption upon statistical properties of wave transport be clari-

fied. In our work we tackle this question by studying the scaling of intensity and transmission distributions in strongly absorbing samples. We find that even strong absorption does not affect substantially the probability distributions of intensity and total transmission. Furthermore, we demonstrate that it is possible to statistically eliminate the influence of absorption upon the statistics of intensity which allows us clarify the interplay between absorption and localization.

3 Total Transmission Distribution in Absorbing Random Waveguides

Fluctuations in transmittance quantities increase dramatically as the ensemble average of the dimensionless conductance, g, approaches unity. Low values of g can be achieved in quasi-one dimensional samples such as conducting wires or multi-mode waveguides with lengths much greater than the transverse dimensions. In this chapter, we report measurements of total transmission of microwave radiation in long waveguides filled with randomly positioned scatterers in which values of the dimensionless conductance as low as $g \approx 3$ are achieved. The distributions are obtained accurately for values of s_a significantly larger than unity which allows us to adequately compare theory and experiment and investigate the number of independent parameters needed to capture the character of the distribution as the sample moves toward the localization transition.

3.1 Background

Nonlocal correlation in the flux transmitted through mesoscopic samples leads to enhanced fluctuations of intensity and spatially averaged transmission for both classical and quantum waves. [71,72] In order to examine the scaling and the universality of transport, therefore, it is important to measure the full distribution of

key transmission quantities as the sample size, and hence g, changes. [4] In previous studies, nonlocal correlation has been shown to lead to higher probabilities at large values of the intensity, leading to a deviation from negative exponential statistics for polarized microwave radiation in samples with $g \sim 10$ [22,65], as well as to discernable deviations from a Gaussian distribution and enhanced variance for the total optical transmission when $g > 10^3$ [47].

Recently, an expression for $P(s_a)$ in terms of g for nonabsorbing samples was obtained by Nieuwenhuizen and van Rossum using diagrammatic techniques combined with random matrix theory [45] and subsequently by Kogan and Kaveh within the framework of random matrix theory. [46] The diagrammatic calculations neglect some terms of order higher than $1/g$, whereas computations based on random matrix theory neglect sample-to-sample fluctuations in the probability distributions of eigenvalues of the transmission matrix and are expected to be accurate only to order $1/g$. More recently, van Langen, Brouwer and Beenakker carried out a nonperturbative calculation of the total transmission distribution in the absence of absorption. [73] An analytic solution is obtained for the case in which time reversal invariance is broken ($\beta = 2$) but not for the case of time reversal symmetry ($\beta = 1$) considered here. However, good agreement is found between the β-independent result for $P(s_a)$ obtained in Refs. [45,46] and the result for $\beta = 2$ in Ref. [73] for $g \geq 10$.

The distribution of total transmission was first measured by de Boer et al. in optical measurements in slabs of titania particles. [47] Samples with $g > 10^3$ were studied and the distribution was found to be Gaussian to within 1%. A measure of

the deviations of the distribution from a Gaussian is the value of the third cumulant $<s_a^3>_c$ which gives the skewness of the distribution and vanishes for a Gaussian distribution. For the samples studied, $<s_a^3>_c$ was of order of 10^{-6}. In this work, we present measurements of the total transmission distribution in samples in which values of g as small as $g \approx 3$ are achieved. The distributions obtained from these measurements are markedly non-Gaussian reaching a value of the third cumulant of approximately 0.1 for the sample with the minimum value of g.

3.2 Samples and measurements

In the present work, low values of g are achieved by placing the sample in a cylindrical copper tube in order to restrict transverse diffusion and thus the number of modes N. The samples consist of polystyrene spheres with diameters of 1.27 cm randomly positioned inside a cylindrical copper tube so that transverse diffusion is restricted leading to a limited number of modes N. Sample tubes with diameters $d = 5.0$ and 7.5 cm and various lengths up to 520 cm are used. Because of the difference in the tube diameters, the samples have slightly different filling fractions of 0.52 and 0.55 for $d = 5.0$ and 7.5 cm, respectively. Measurements are made in the frequency range 16.8 - 17.8 GHz using frequency steps of 4 MHz. The sample tube is rotated between successive measurements to produce new scatterer configurations. In order to eliminate the instrumental response, the spectra are normalized to their ensemble average to give s_a from which the distribution $P(s_a)$ is obtained. The microwave radiation is coupled to the sample by a 0.4 cm wire antenna placed 0.5

cm from the front surface of the sample and the total transmission is measured by use of a Schottky diode detector positioned inside an integrating sphere rotating about the sample axis at 2 Hz. A schematic diagram of the experimental set up is shown in Fig. 8. The integrating sphere has a diameter of 40 cm and is comprised of two concentric plastic spherical shells separated by 2 cm with the space between them filled with movable scatterers. The outer shell is covered with aluminum foil to form an irregular reflecting surface. The region between the shells is filled with aluminum cylinders with diameters of 0.75 cm and typical lengths of 1 cm. The cylinders tumble as the integrating sphere rotates resulting in a fluctuating intensity at the detector with a correlation time of $\sim$ 2 ms for the sample with a length of 100 cm. The signal is averaged for 1 s at each frequency giving an uncertainty of 2.5 % in the measurement of transmission. At the maximum length of 200 cm at which total transmission measurements were made, a traveling wave tube amplifier (TWTA) with an output power of 40 W is used. The transmission distributions are obtained by using the data from at least 1000 sample configurations.

In the frequency range of the measurements, $\ell \sim 5$ cm [74]. A fit of measurements of the field autocorrelation function with frequency shift to theory [63] gives $L_a = 34 \pm 2$ cm and $D = (3.03 \pm 0.21) \times 10^{10}$ cm^2/s. [75] The localization length for the samples with $d = 5$ cm is found to be $\xi = 551 \pm 18$ cm from field measurements [48] which will be discussed in the next chapter.

3.3 Results and discussions

From the measurements of total transmission made, we obtain the probability distribution $P(s_a)$. The distributions for three samples with dimensions (a) $d = 7.5$ cm, $L = 66.7$ cm, (b) $d = 5.0$ cm, $L = 50.0$ cm, and (c) $d = 5.0$ cm, $L = 200$ cm are shown in Fig. 9. In the absence of absorption, the dimensionless conductance for these samples without localization corrections, $g = N\ell/L$, would be approximately 15.0, 9.0, and 2.25 for samples a, b, and c, respectively. The distribution broadens and the deviation from a Gaussian becomes more pronounced as either the sample length increases or the cross-sectional area decreases. A value of $<s_a^3>_c$ as large as 0.112 ± 0.035 is observed for sample c. Deviations from a Gaussian distribution in the tail of the distribution for this sample can be seen in the semilog plot of $P(s_a)$ in Fig. 10. For values of $s_a \geq 2$ the distribution is essentially exponential.

We compare the theoretical results from Refs. [45,46] to the measured transmission distributions. The full distributions are given by the theory as functions of g for nonabsorbing samples. In the present case of strong absorption, the photon number is not conserved and g cannot be defined in terms of the steady state transmission, while serving as a useful measure of the proximity to the localization transition. This can be seen by noting that the reduction of the average transmission due to the presence of absorption is associated with a decrease rather than an increase of the degree of correlation in the sample and to push the system farther from the localization threshold. A parameter which characterizes the transmission distribution as well as the closeness to the localization threshold is the degree of cor-

relation of intensity in different coherence areas of the transmitted speckle pattern, $<\delta s_{ab}\delta s_{ab'}>$. Were this correlation to vanish, fluctuations in different coherence areas would be independent and the transmission distribution would be Gaussian as required by the central limit theorem, with $var(s_a) \equiv <s_a^2>_c = 1/N$. As a result of nonlocal correlation, however, the variance of the transmission is enhanced. It is given by $var(s_a) = (var(s_{ab}) - 1)/2 = <\delta s_{ab}\delta s_{ab'}>$. [17,19,46,62] The last equality is consistent with the results of Ref. [62] when the cumulant intensity correlation function is properly normalized to the renormalized average transmission. [63] In that case, the crossing parameter found by Shnerb and Kaveh [64] which determines the intensity distribution is found experimentally to be equal to $<\delta s_{ab}\delta s_{ab'}>$. [62,65] In independent measurements with the sample with $L = 100$ cm and $d = 7.5$ cm, we find that the intensity correlation function with space shift Δx has a constant value of 0.0646 ± 0.0012 for $\Delta x > 3$ which equals within experimental error the value of $var(s_a) = 0.0656 \pm 0.0020$ for this sample. [75] The connection between $<\delta s_{ab}\delta s_{ab'}>$ and the full transmission distribution can be seen by considering the expression of Refs. [45,46] for $P(s_a)$ in the absence of absorption in the limit $g \gg 1$,

$$P(s_a) = \int_{-i\infty}^{+i\infty} \frac{dx}{2\pi i} exp[xs_a - \Phi(x)], \tag{18}$$

where

$$\Phi(x) = gln^2(\sqrt{1 + x/g} + \sqrt{x/g})$$

is the generating function. From Eq. (18) one obtains the expression for $var(s_a)$ in terms of g,

$$var(s_a) = \frac{2}{3g}. \tag{19}$$

From these expressions, a general relation for $P(s_a)$ in terms of $var(s_a)$, or equivalently $<\delta s_{ab}\delta s_{ab'}>$, can be found by using Eq. (19) to define a new parameter $g' = 2/3var(s_a)$ which is substituted for g into Eq. (18). Plots of $P(s_a)$ obtained by following this procedure with g' determined from the measured values of $var(s_a)$, are shown as the solid lines in Figs. 9 and 10. We find that $P(s_a)$ is accurately given even for the lowest value of g' of 3.06 (sample c). The distribution of Eq. (18) with g' substituted for g gives the exponential tail, $P(s_a) \sim exp(-g's_a)$ in the limit $s_a \gg 1$. For $s_a \geq 2.0$, the linear fit to the logarithm of the measured transmission distribution for sample c gives a slope of $-(2.71 \pm 0.06)$ in accord with the fit of an exponential function to the theoretical curve gives a slope of - 2.70 in this range and is close to its predicted asymptotic value of 3.06 for $s_a \gg 1$.

The extent of the agreement of Eq. (18) when g' is substituted for g can also be gauged from the comparison between the calculated (circles) and the measured (squares) moments of the transmission distribution shown in Fig. 11 for samples with $g' = 10.2 \pm 0.1$ and $g' = 3.06 \pm 0.04$. The moments calculated from the theory are close to those obtained from the measured distributions. At $n = 10$, these differ by approximately 10 % which is within the experimental error. Thus it appears that $P(s_a)$ can be expressed as a function of the parameter $var(s_a)$.

The agreement between theory and experiment indicates that the ratio of moments is accurately reflected in Eq. (18). The dependence of the variance itself

upon sample dimensions is shown in Fig. 12. In the limit of $g \gg 1$ in the absence of absorption and internal reflection $var(s_a) = 2L/3N\ell$. The straight line in the figure is drawn through the first data point and represents $var(s_a) \sim L/\xi$. As $g \rightarrow 1$, the scaling theory of localization [40] suggests that g falls exponentially and hence $var(s_a)$ should increase superlinearly with sample length. Instead, we find, that $var(s_a)$ depends sublinearly upon L. This is presumably due to the presence of absorption which diminishes the degree of nonlocal correlation. This raises the question of whether the transmission distribution continues to broaden as L increases or instead it reaches a limiting distribution for particular sample parameters.

3.4 Conclusions

In conclusion, we have measured the total transmission distribution of microwave radiation in quasi-one dimensional absorbing samples with small values of g. We find that the distribution can be described using an expression originally derived for nonabsorbing samples in the limit $g \gg 1$ when this expression is reformulated as a function of the single parameter $g' = 2/3var(s_a)$ determined from the measurements. The validity of the expression for values of g' as small as 3, well beyond the limits assumed in the calculations, may well be associated with the identification of $var(s_a)$ with $<\delta s_{ab}\delta s_{ab'}>$, the degree of spatial correlation in the sample, which is the key microscopic parameter in mesoscopic physics. The sublinear increase of $var(s_a)$ with L in strongly absorbing samples, however, raises the question as to

whether radiation can be localized in the presence of absorption.

4 Intensity Distribution in the Approach to Localization

In this chapter, we focus on the intensity distribution, which is the key distribution in statistical optics. [3] We demonstrate its relationship to the distribution of total transmission, find the scaling of the variance of the intensity and total transmission up to $L = \xi$, and determine the extent to which absorption influences localization.

4.1 Background

In the diffusive limit, the degree of long-range intensity correlation is small and the intensity distribution is well approximated by the Rayleigh distribution. [3,22,76] For polarized detection, this corresponds to negative exponential statistics, $P(s_{ab}) = exp(-s_{ab})$. In previous work, deviations from negative exponential behavior have been observed and ascribed to long-range intensity correlation [22,64,65]. In these studies [22,65], fluctuations as large as $s_{ab} \sim 10 \sim g$ were observed. In the present work, fluctuations as large as fifty times g are observed in samples with lengths $L \sim \xi$.

The intensity distribution is studied in a quasi-1D geometry, which is equivalent to the electronic case of a thin wire. Thouless argued that, the level width $\delta\nu$

in a wire at $T = 0$ should become smaller than the level spacing $\Delta\nu$ since $\delta\nu$ is proportional to the inverse of the travel time and so falls as $1/L^2$ in the diffusive limit, whereas $\Delta\nu$ is the inverse of the density of states and so falls as $1/L$. As a result, the modes in adjacent sections of the wire should not overlap, and electrons should become localized. [39]

The question arises as to whether radiation can be localized in the presence of absorption. In this case, the level width falls as $1/L$, just as the level spacing does. In the previous chapter, we showed that the variance of the normalized total transmission, $var(s_a)$, scales sublinearly with L in the presence of absorption. If the attenuation length due to absorption, L_a, serves as a cutoff length for localization [26,32] then $var(s_a)$ would approach an asymptotic limit as L increases. On the other hand, if localization can be achieved in absorbing samples, then $var(s_a)$, which is essentially the degree of correlation in the intensity of different outgoing modes, should increase superlinearly as L approaches ξ. This might occur, since the wave remains temporally coherent in the presence of absorption. [77,78] Weaver has shown in a 2-D simulation that the introduction of absorption does not disrupt the spatial localization of acoustic waves in closed systems, though the overall energy decreases exponentially with time. [77] In recent calculations, Brouwer found that for diffusive waves the prefactor multiplying L/ξ in the expression for $var(s_a)$ drops from $\frac{2}{3}$ to $\frac{1}{2}$ as the ratio L/L_a increases. [79] The behavior of this quantity, however, was only considered for lengths considerably less than the localization length.

Here we report measurements of intensity transmitted through random waveg-

uides with $L \leq \xi$, but $> L_a$. We expect that modes in this sample are completely mixed and the degree of intensity correlation between different modes is constant. Wave propagation in this sample should therefore be described by random matrix theory (RMT). [61] Recently, Kogan and Kaveh used RMT to obtain a relationship between the moments of intensity and total transmission in nonabsorbing quasi-1D samples. [46] They find,

$$<s_{ab}^n> = n! <s_a^n>, \tag{20}$$

This leads to a relationship between the distributions of intensity and total transmission, [46,80]

$$P(s_{ab}) = \int_0^\infty \frac{ds_a}{s_a} P(s_a) exp(-\frac{s_{ab}}{s_a}). \tag{21}$$

Since the distribution of total transmission can be calculated from the distribution of the eigenvalues of the transmission matrix, [45,46,73] these relations provide a basis for calculating the intensity moments and distributions from RMT.

4.2 Samples and measurements

The samples used in the measurements of the intensity distributions are the same as those described in the previous chapter. Here, however, measurements of intensity were made for sample lengths as large as 520 cm ($\sim \xi$). Different sample configurations are created as in the case of total transmission measurements by briefly rotating the sample tube between successive measurements. At least two thousand sample configurations were used for each distribution. Field spectra were

taken from 16.8 to 17.8 GHz in steps of 1 MHz using a Hewlett-Packard 8722C network analyzer. The radiation is coupled into and out of the sample by 0.4 cm wire antennas placed 0.5 cm from the ends of the sample. Schematic diagram of the experimental set up is shown in Fig. 13. In order to ensure that the distributions were not distorted by noise, it was necessary to use an amplifier with an output power of 40 W for samples with lengths greater than 200 cm so that the average intensity was at least three hundred times the noise.

4.3 Results and discussions

In Fig. 14, we present the intensity distributions for two samples with $L/\xi \sim 0.1$ and 0.4. Calculations for diffusive waves in the absence of absorption have predicted that for $s_{ab} \gg g$, the intensity distribution falls as $exp(-2\sqrt{gs_{ab}})$. [45] For the samples measured, we find $P(s_{ab}) \sim exp(-2\sqrt{\gamma s_{ab}})$ in the tail of the intensity distribution. The values of γ obtained from a fit to the tail of the measured distributions is within 20% of the parameter $g' = \frac{2}{3var(s_a)}$, [43] which equals g in the absence of absorption . The fit of a negative stretched exponential to the distribution for $L/\xi = 0.4$ in the range of s_{ab} from 10 to 18 is shown in Fig. 15 and gives $\gamma = 2.9$, which is close to value of g' of 3.06 for this sample.

The measured intensity distributions are compared to the transform of the measured transmission distributions [43] for the corresponding samples using Eq. (21). The transforms shown as solid lines in Fig. 14, are in good agreement with the

measured intensity distributions. A comparison of the moments of intensity and transmission is shown in Fig. 16. We find an increasing deviation of the ratios $<s_{ab}^n> /n! <s_a^n>$ from the value of unity expected from Eq. (20) as n increases. We find, however, that agreement with Eq. (20) is dramatically improved when the moments are calculated using the asymptotic expressions in the diffusive limit for the intensity and transmission distributions beginning from the point at which the measured distribution have their first zero. The asymptotic expressions for the intensity distribution $exp(-2\sqrt{g's_{ab}})$ is substituted for the measured distribution for values of s_{ab} between20 and 150, whereas the asymptotic exponential expression $exp(-g's_a)$ [43,45,46] is substituted for the measured transmission distribution for values of s_a between 5 and 25. The improved agreement indicates that the extent to which the measured ratio of moments is in accord with Eq. (20) is largely limited by the range of intensity and transmission values measured, which depends on the number of configurations on which measurements were made.

Applying Eq. (20) to the second moments gives

$$var(s_{ab}) = 2var(s_a) + 1. \tag{22}$$

The same expression can be obtained from a perturbation calculation up to order $1/g$ [17,46]. Our measurements confirm the prediction of RMT that Eq. (22) is independent of the value of g and is correct up to order 1/N. In Fig. 17 we plot the ratio $var(s_{ab})/[2var(s_a) + 1]$ obtained from the measurements of total transmission and intensity. For all samples for which this comparison is possible agreement to

within 3% is found between experiment and theory (Eq. (22)).

Intensity statistics at the localization threshold are studied in measurements at $L = 520$ cm and $d = 5$ cm ($L/\xi \sim 1.0$) and shown in Fig. 18. Values of s_{ab} as large as 50 are observed. The distribution for this sample is seen in Fig. 19a to be nearly log-normal, in agreement with predictions for localized radiation [73,79]. A comparison to the distribution obtained for a sample with $L/\xi \sim 0.1$ (Fig. 19b) indicates the transition to a log-normal distribution as $L/\xi \rightarrow 1$.

Using Eq. (21), we compare these measurements of the intensity distribution to random matrix calculations of the transmission distribution in the presence of absorption [79]. In order to compare the intensity distribution to theory, however, ξ must be determined. We recall, that far from the localization threshold, in the absence of absorption and internal reflection, $var(s_a)$ and ξ are related by Eq. (19) [17,45,46,79].

To find ξ in samples in which corrections due to absorption, localization and internal reflection cannot be ignored, we first obtain the intensity distribution for the equivalent samples without absorption using the measured spectra in our absorbing samples. We first obtain the time response $E(t)$ to a narrow Gaussian pulse in time by Fourier transforming the product of the measured spectrum and a broad Gaussian in the frequency domain. The time dependent field is then multiplied by $exp(t/2\tau_a)$, where $\tau_a = {L_a}^2/D = (3.81 \pm 0.70) \times 10^{-8}$ s is the exponential attenuation time due to absorption. The modified time spectra are then transformed back into the frequency domain. The spectra in frequency and in time domain as obtained

from the measurements (thick line) and as corrected for absorption (thin line) are shown in Fig. 20. The peaks in the frequency spectrum obtained after correcting for absorption are clearly narrower as compared to those observed in the measured spectrum. This is consistent with the affect of absorption which reduces the average dwell time of photons and thus broadens the level width of modes. From the field spectra corrected for absorption, we now obtain intensity distributions. In Fig. 21. we compare these with the measured distributions. At high intensity values. the measured distribution appears lower than the one obtained from the data corrected for absorption. This is consistent with the influence of the presence of absorption upon intensity statistics. The intensity distributions obtained in this way are in good agreement with transforms of the diffusive result for the distributions of total transmission calculated in Ref. [45,46] (see the insert in Fig. 21) and give values for the parameter g' [43] equal to the value of g, as expected in the absence of absorption. We also find that the average transmission obtained from the spectra corrected for absorption is consistent with the expected scaling as $(L + 2z_b)^{-1}$. . where z_b is the diffusion extrapolation length due to internal reflection [81]. These results confirm the ability of this approach to statistically eliminate absorption in the diffusive limit. We do not expect the procedure to be effective for localized waves. In this case, the presence of gain is predicted to lead to an overall suppression of transmission, [82,83] whereas an extension of the present approach would lead to enhanced transmission. This indicates the importance of dispersion as well as amplification or loss in this case. The influence of internal reflection upon $var(s_a)$

in the absence of absorption can be accounted for by substituting $\tilde{L} = L + 2z_b$ for L in Eq. (19). We next account for the leading order correction to $var(s_a)$ due to nonlocal correlation. In the absence of absorption, the variance is increased by an additional factor of $(1 + \frac{2\tilde{L}}{5\xi})$ [63,84] to yield,

$$var(s_a) = \frac{2\tilde{L}}{3\xi} + \frac{4\tilde{L}^2}{15\xi^2}. \tag{23}$$

A fit of Eq. (23) to the data corrected for absorption using ξ and z_b as fitting parameters gives $\xi = 551 \pm 18$ cm and $z_b = 5.25 \pm 0.31$ cm. The value of z_b obtained is consistent with the values of this parameter for the same samples in the frequency range between 18 and 19 GHz. [74]

The dependence of $var(s_a)$ upon L with and without absorption is shown in Fig. 22. The solid curve represents the result of the calculations in the diffusive regime ($L/\xi \ll 1$) by Brouwer [79] which account for absorption and the dashed curve shows the fit of Eq. (23) to the data corrected for absorption. The values of $var(s_a)$ are calculated from $var(s_{ab})$ using Eq. (22). For lengths up to 200 cm, the result from the measurements, show sublinear behavior which is consistent with the results from total transmission measurements [43] and the calculations in Ref. [79]. The deviation from the solid line increases for larger lengths and may reflect localization corrections that were not included in the theory. For strongly absorbing samples ($L \gg L_a$), Brouwer finds a log-normal distribution for the total transmission with $<lnT_a>= -L/L_a - 3L/4\xi - lnN$ and $var(lnT_a) = L/2\xi$. [79] This allows us to calculate the values of $var(s_a)$ for the two samples with $L \geq 10L_a$ for which

measurements were made. These are presented as the squares in the figure and indicate significant corrections due to localization in qualitative agreement with the results from the measurements. Thus, we can associate the increase of $\xi var(s_a)/\tilde{L}$ for these samples with the transition to localization.

We now compute $P(s_{ab})$ for the sample with $L = 520$ cm using the transmission distribution calculated in Ref. [79] and the values of ξ and L_a found here. The calculated intensity distribution is presented as the solid line in Fig. 18 and is in good agreement with the measurements.

We also test the extent to which the theoretical calculations in the diffusive limit and in the absence of absorption [45,46] agree with the measurements for this sample for which $L/\xi \sim 1$ and $L/L_a \approx 15$. Using Eq. (18), we calculate $P(s_a)$ with g' obtained from the measured variance of intensity. The calculated transmission distribution is then transformed to give the corresponding intensity distribution which is shown by the dashed line in Fig. 18. Surprisingly, even in the presence of strong absorption and at the localization length the diffusion theory in the absence of absorption when properly modified (the distribution obtained from theory is calculated so that it has the right variance) still provides good agreement with the experiment. A comparison with the calculations in which absorption and localization corrections are included (the solid line in the figure) shows deviation between these two results only for large values of intensity. In contrast, the transmission distributions from which the intensity distributions are calculated can be visibly set apart (see the insert). In order to describe quantitatively the difference between

these two results, one has to consider higher moments in total transmission (or intensity). The diffusion theory in the absence of absorption predicts that the ratio $C(L) = <s_a^3>_c / var(s_a)^2$, where $<s_a^3>_c$ is the third cumulant of the distribution, has a constant value of 12/5 in the case of an incident plane wave. [45] In RMT calculations in the diffusive limit in which absorption is included, Brouwer found that the value of this parameter changes from 12/5 in the absence of absorption to 3 in strongly absorbing samples. [79] In Fig. 23, we plot the values of C(L) obtained from the intensity measurements via Eq. 20 which show a qualitative agreement with the theoretical result of Brouwer (solid curve). Because of the small values of $<s_a^3>_c$ for samples with small L (large values of g), the error bar in the results from the measurements is very large and a quantitative comparison with theory is not possible. For $L \sim \xi$, however, the value of the third cumulant increases and the accuracy of the experimental results is improved significantly. For these samples, we find values of $C(L)$ greater than the theoretically predicted value of 3. This can be associated with the approach to localization. We calculate $C(L)$ using the expressions for the total transmission from Ref. [79] in which localization corrections are included. The results are shown as squares and, as in the case of $var(s_a)$, show the same trend which is found in the experiment.

4.4 Conclusions

In conclusion, we find that the intensity distribution for $s_{ab} \gg g$ is described by a negative stretched exponential to power 1/2 and that the distribution for $L \sim \xi$ is close to log-normal. We confirm experimentally the relationships obtained by Kogan and Kaveh between the moments and full distributions of intensity and total transmission. These relations unify the statistical description of local and spatially averaged transmittance quantities. Our measurements demonstrate that the statistics of wave transport is only marginally affected by absorption and that absorption does not substantially inhibit localization. The ability to reach the localization threshold using a quasi-one-dimensional sample is an extension to classical waves of the suggestion by Thouless that electrons will always be localized in sufficiently long wires at low temperatures. These results show that the variances of the intensity or transmission are reliable measures of the impact of localization upon transport in random media.

5 Field and Intensity Correlations in Random Waveguides

In this chapter we obtain the absorption length and the diffusion constant of the samples discussed in chapters 3 and 4 from the field auto correlation function with frequency shift. We show also that the variance of the total transmission equals the degree of nonlocal intensity correlation across the output face of the sample. Finally, we present measurements of the long- ($C2$) and infinite-range (C_3) terms of the intensity correlation function with frequency shift. To the best of our knowledge, measurements of the frequency dependence of the C_3 correlation term are reported for the first time in this work.

5.1 Field-field correlation function with frequency shift

The field autocorrelation function with frequency shift $\delta\omega$ is defined as $<I(\omega,\Delta\omega)>=<E(\omega)E^*(\omega+\Delta\omega)>$. It reflects the short-range intensity correlation which is simply $C_1(\omega,\Delta\omega) =|<I(\omega,\Delta\omega)>|^2$

Inside the sample

$$<I(\mathbf{r},\omega,\Delta\omega)>= \frac{sinh[(\gamma_+ - i\gamma_-)(L-z)|}{sinh[(\gamma_+ - i\gamma_-)L|}, \tag{24}$$

where $\gamma_\pm^2 = \sqrt{\alpha^4+\beta^4} \pm \alpha^2$, $\alpha = L_a^{-1}$ is the absorption coefficient, and $\beta = (\Delta\omega/D)^{1/2}$. [63] For samples for which $\alpha\ell$, $\beta\ell \ll 1$ and $z_b \approx \ell$ the field auto corre-

lation function at a point at the output face of the sample is given by

$$<I(\omega,\Delta\omega)>=\frac{sinh[(\gamma_+-i\gamma_-)z_b]}{sinh[(\gamma_+-i\gamma_-)L]}\approx\frac{(\gamma_+-i\gamma_-)z_b}{sinh[(\gamma_+-i\gamma_-)L]}. \quad (25)$$

When the function is normalized to the outgoing average intensity

$$<\tilde{I}(\omega,\Delta\omega)>=\frac{\gamma_+-i\gamma_-}{\alpha}\frac{sinh(\alpha L)}{sinh[(\gamma_+-i\gamma_-)L]}. \quad (26)$$

We obtain $<\tilde{I}(\omega,\Delta\omega)>$ from the measurements from which the intensity distributions (discussed in chapter 4) were obtained. In Fig. 24 we present its real part for the sample with $L/\xi\approx 0.1$. From a fit of Eq. (26) to the data, using α and D as fitting parameters, we obtain $L_a = 34\pm 2$ cm and $D = (3.03\pm 0.21)\times 10^{10}$ cm^2/s. The result from the fit is shown on the plot as a solid line.

5.2 Intensity-intensity spatial correlation function

In this section we demonstrate experimentally that the variance of the total transmission distribution equals the degree of nonlocal correlation across the output face of the sample. In microwave measurements of the intensity distribution and the intensity-intensity correlation function with frequency shift, Genack and Garcia have shown that the variance of the distribution is directly related to the $C^x(\equiv C_2+C_3)$ term of the correlation function at zero frequency shift which represents the degree of nonlocal intensity correlations in the system. [65,62] Here we confirm this relation in a more direct way by measuring the intensity-intensity correlation function with displacement.

This is done by measuring the transmitted field as the detecting antenna is moved to different positions along the diameter of the sample output. The intensity-intensity correlation function, $C_{\omega\omega'}(\mathbf{r},\mathbf{r}') \equiv <\delta I_\omega(\mathbf{r})\delta I_\omega(\mathbf{r}')>$, consists of three contributions $C = C_1 + C_2 + C_3$. For two observation points at the output plane which are separated by a distance ΔR, the short-range part C_1 is given by [63]

$$C_{1\omega\omega'}(\mathbf{R},\mathbf{R}') = |<I_{\omega\omega'}(\mathbf{R})>|^2 \left[\frac{sin(k_0\Delta R)}{k_0\Delta R}\right]^2 exp(-\Delta R/\ell), \tag{27}$$

where k_0 is the wave number in air and ΔR is the distance between the two points of detection. Normalizing to the outgoing average intensity and taking $\omega = \omega'$ leads to

$$C_1(\mathbf{R},\mathbf{R}') = \left[\frac{sin(k_0\Delta R)}{k_0\Delta R}\right]^2 exp(-\Delta R/\ell). \tag{28}$$

The long-range term, C_2, in the intensity-intensity correlation function also depends on the displacement. In the quasi-1D geometry, however, this term is dominated by the zero-mode contribution which is spatially independent and is equal to the relative fluctuations in total transmission ($var(s_a)$). [63] The C_3 term is of order $1/g^2(\ll 1)$ and is considered to be constant.

The intensity correlation function with displacement is obtained for the polystyrene sample with $L/\xi \sim 0.1$. The transmitted field is measured as the position of the detecting antenna is changed in steps of 1 mm to cover a distance of 5 cm across the output face of the sample. Field spectra between 16.8 and 17.8 GHz are taken for each sample configuration and for each position of the detecting antenna. Measurements are made for 600 different sample configurations. From the

data we obtain the intensity-intensity correlation function with displacement (Fig. 25) We fit the expression for $C(\Delta R) = C_1 + \tilde{C}_2$ with C_1 given by Eq. (28) and $\tilde{C}_2$ = constant to the experiment. The term $\tilde{C}_2$ represents the spatially independent part of C_2 and includes the infinite-range correlation (C_3) term as well. We use k_0, ℓ, and $\tilde{C}_2$ as fitting parameters. The result of the fit is presented on the plot by a solid line. We note that the value of $k_0 = 4.22$ obtained from the fit gives an index of refraction $n = 1.16$ which is between the value of n in air and the effective index of refraction in the sample of $n \approx 1.35$. This can be associated with the fact that close to the output face of the sample, the speckle pattern has already begun to "broaden" as compared to the picture inside and its characteristic length is different from the wavelength in the sample. The value of the constant term, however, is not affected in any way. We obtain $\tilde{C}_2 = (6.46 \pm 0.12) \times 10^{-2}$ which, within experimental error, equals the value of the variance of the total transmission for this sample, $var(s_a) = (6.56 \pm 0.20) \times 10^{-2}$. The excellent agreement between the results of these independent measurements (we recall that $var(s_a)$ is obtained from the measurements of total transmission distributions) confirms that $var(s_a)$ is given by the degree of nonlocal correlation. In light of the results presented in the previous chapter, this indicates that the degree of nonlocal intensity correlation is a key parameter which determines the statistics of mesoscopic transport.

5.3 Total transmission measurements of long- and infinite-range intensity correlation

Here we present measurements of the C_2 and C_3 terms of the intensity correlation function with frequency shift. Although the analysis of the results from these measurements are still in progress, we present our results, because of the significant interest toward these quantities. C_3 is of particular interest, since it is the analog of UCF in the case of classical waves. The frequency dependence of the long- (C_2) and infinite-range (C_3) correlation terms has been considered in various theoretical works (for a comprehensive review on the subject we refer to the work of van Rossum and Nieuwenhuizen [86] and the references therein) and the frequency dependence of C_2 has been observed experimentally [62,65]. In these experiments, however, the contribution of C_3 in the intensity correlation function was found to be small as compared to the other terms and in the analysis of the data was considered to be frequency independent. In measurements of total transmission we obtain the cross-correlation function between two input modes with frequency shift in which the C_3 term is dominant. [75]

Total transmission measurements with a polystyrene sample with $L/\xi \sim 0.1$ are made as described in chapter 3. In order to observe the infinite-range correlation, however, two identical wire antennas are used as independent sources of excitation. These were placed 0.5 cm in front of the input face of the sample and were separated by a distance of 3.0 cm which is approximately twice the wavelength. Transmission spectra for a single sample configuration are taken separately for each antenna by

using a microwave switch which couples radiation to one of the antennas only while isolating the other. Measurements for four thousand sample configurations were made. From these measurements, we obtain the autocorrelation function in total transmission with frequency shift using spectra taken with the same antenna and the cross-correlation function between spectra taken with different antennas.

We first turn our attention to the total transmission autocorrelation function which is shown in Fig. 26. It is much broader as compared to the intensity auto correlation function (which is dominated by the short-range correlation term) which explains the difference between the average peak width in intensity and total transmission as discussed in the beginning of chapter 2.

To order $1/N$, the total transmission autocorrelation function equals the C_2 term of the intensity auto correlation function. In the presence of absorption this term is given by [85]

$$C_2(\Omega) = \frac{3\pi}{2\alpha^2 \ell A}(cos(2bL) - cosh(2aL))^{-1} \times [\frac{\alpha^2 - 2a^2}{a(a^2-\alpha^2)} sinh(2aL) + \frac{\alpha^2 + 2b^2}{b(\alpha^2+b^2)} sin(2bL) + \frac{\alpha^2(a^2+b^2)}{(a^2-\alpha^2)(\alpha^2+b^2)} sinh(2\alpha L)|, \quad (29)$$

where $\Omega = \Delta\omega/D$, $a = (\alpha^4+\Omega^2)^{\frac{1}{4}} cos(\varphi/2)$, $b = (\alpha^4+\Omega^2)^{\frac{1}{4}} sin(\varphi/2)$, and $tan\varphi = \frac{\Omega}{\alpha^2}$. As before, the role of internal reflection is accounted for by substituting $\tilde{L} = L + 2z_b$ for L in this expression. We calculate $C_2(\Omega)$ from Eq. (29) using the values of L_a and D determined from the field autocorrelation function. The result from the calculations is presented by the solid line in Fig. 26 and shows good agreement with experiment. Only for large frequency shift slight deviations between theory

and experiment are observed. We plot also the theoretical curves in the absence of absorption and internal reflection (dashed line) and when absorption is included only (dotted line). The comparison shows that absorption affects C_2 in two ways: first, it decreases the magnitude of the degree of long range correlation ($C_2(0)$) which is consistent with the results for $var(s_a)$ in chapters 3 and 4 [§]; second, the presence of absorption broadens the frequency width of the correlation which is associated with the reduction of the average dwell time of photons in the sample.

Finally, in Fig. 27a, we plot the cross-correlation function with frequency shift obtained from these measurements. We find that its value at zero frequency shift of is comparable to the value of $2/15g^2$ as predicted by theory [62,87]. The behavior of the total transmission cross-correlation function measured is in qualitative agreement with the theoretical calculations by van Rossum et al. [87] in the presence of absorption (Fig. 27b). A detailed quantitative analysis considering the contribution of long-range correlation which are expected to be comparable to the C_3 contribution in the measured cross-correlation function are in order.

[§]When we used Eq. (29) to calculate $C_2(0)$ in the presence of strong absorption, we found the same reduction from 2/3 to 1/2 as predicted by Brouwer [79].

6 Microwave Transmission Through a Periodic 3D Metal Wire Network Containing Random Scatterers

6.1 Background

Band gaps exist in the electromagnetic spectrum in a variety of periodic structures in analogy with the electronic band gaps in crystals [33,49,50]. In the photonic band gap (PBG), electromagnetic waves are evanescent. When disorder is introduced in a PBG structure, modes can be created into the gap but they are localized and again propagation is inhibited. Such localized states could be associated with a single defect in the photonic crystal which are analogous to localized electron states on isolated impurities in semiconductors [88] or to localized vibrational modes associated with defects in crystals [89,90]. They may also be associated with scattering from a statistically homogeneous random distribution of scatterers. John predicted the existence of a mobility edge separating localized from propagating electromagnetic waves within the pseudogap for nearly periodic systems [49]. He proposed that introducing disorder would lead to strong Anderson localization for photons [34]. In the present study, we measure transmission through a nearly periodic copper wire network with a structure close to simple cubic. A PBG is found in this structure both when it is empty and when it is filled with Teflon spheres producing a Teflon-air medium. By substituting aluminum spheres for some of the Teflon spheres, we

create a succession of random scatterer configurations inside the structure. The transmission is measured in an ensemble of random scatterer configurations for various degrees of disorder introduced within the periodic metal matrix. The band structure for various 3D dielectric [50–53] and metallic [54–56] periodic structures possessing band gaps have been calculated and dielectric [50,57–59] and metallic [60] systems possessing band gaps have been constructed. Localized states have been created by adding to, removing or displacing part of the structure in dielectric PBG materials and by cutting selected wires in metal systems [58,60]. These defects are introduced in a controlled manner so that it is possible to associate specific modes with particular defects. Our interest here is to create an ensemble of equivalent random configurations of scatterers within the PBG structure. We introduce disorder in a nearly periodic metal wire network by filling it with mixtures of Teflon and aluminum spheres. The Teflon and aluminum spheres have diameters of 0.47 cm. This is approximately half the lattice constant of the wire network of $a = 1$ cm and the spheres readily penetrate the interior of the wire structure. The Teflon sphere medium has a scattering length which is much greater than the dimensions of the metal structure. Consequently, the Teflon spheres serve as an ideal support matrix into which scatterers can be substituted.

Sigalas et al. calculated the band structures for 3D periodic metal systems consisting of isolated metal scatterers and of metal wires which form a continuous network [56]. Periodic systems composed of isolated metal scatterers show behavior similar to that of dielectric PBG materials and do not exhibit a cutoff frequency

below which transmission is sharply reduced. Calculations for metal networks with simple cubic and diamond type structures predict a PBG in both systems. The cubic structure considered is infinite along the x and y directions and has a thickness along the z-axis of $L = 4a$ with a lattice constant a of 1.27 μ m. The volume fraction occupied by the metal wires is 0.03. A band gap is found below a cutoff frequency $\nu_c = \gamma c/a$, where c is the speed of light in vacuum and $\gamma = 0.4445$. At $\nu_c/2$, the attenuation is approximately 15 dB per unit cell.

6.2 Samples and measurements

The metal structure used in our experiment is a network of 1 mm diameter copper wires. The system has a geometry close to simple cubic structure with a lattice constant of 1 cm. The sample has a length of 8 cm on each side. Square wire meshes are created by overlaying one set of parallel wires onto another set of parallel wires oriented in the perpendicular direction. Straight wires are extended through parallel 2D wire meshes in the longitudinal direction. Wires oriented in the three direction are connected by a light solder applied at the vertices of the unit cells. The lattice is not perfectly periodic because of slight bending of the wires and because of variations in the solder joints. The volume of the copper wires is 6 % of the total volume of the system. The front and back of the structure are open and copper plates are placed on the sides.

The transmission is measured in the frequency range between 4.0 and 10.4 GHz using a Hewlett-Packard 8722C network analyzer. Antennas, consisting of 1.5 cm

pins, coupled the radiation to the metal network and detected the transmitted radiation. The input antenna and the front surface of the network are enclosed in an absorbing chamber and the detector and the output surface of the sample are within another chamber with absorbing walls. The antennas were placed 0.5 cm from the input and output faces of the sample. They are placed close to the sample to enhance the signal so that the measurements can be performed with an adequate dynamic range. As a result, however, the incident and detected waves cannot be approximated by plane waves.

6.3 Results and discussions

The results of the measurements in an empty metal network are shown in Fig. 28a. There is a sharp reduction in the transmission coefficient at a cutoff frequency of 9.33 GHz. This gives $\gamma = 0.31$ for the constant of proportionality in the relation $\nu_c = \gamma c/a$. There is a difference between the value of γ observed and the value calculated theoretically [56] which maybe due to the difference in the filling fractions of metal wires in the sample used in the experiment and in the theoretical model. For frequencies below ν_c, the transmission is significantly suppressed. The average value of the attenuation in the gap from 6 GHz to ν_c is approximately 30 dB. At frequencies around 5 GHz, however, a transmission peak occurs in which attenuation is reduced to approximately 10 dB. This peak in transmission may arise because of deviations of the structure from simple cubic symmetry or it may be associated with surface sates [91]. The sharp peaks in the spectrum observed above the cutoff

frequency are a result of the interference between partial waves propagating through the system and reaching the detecting antenna. When the antennas are far from the sample only modes with small transverse components of the wave vector are detected and the spectrum appears relatively flat above the gap.

When the network is filled with Teflon spheres at a volume filling fraction of 0.57 which is measured as a fraction of the total volume free of metal, the cutoff frequency shifts to 7.58 GHz (Fig. 28b). The frequency of the transmission peak in the gap undergoes the same fractional shift. This confirms that the peak is intrinsic to the metal structure. Since $\nu_c \sim v_{ph}/a$, where v_{ph} is the phase velocity in the medium , we expect that the fractional shift of the cutoff frequency is proportional to the ratio of the phase velocities in air and in the medium of random Teflon spheres and air.

In order to determine the phase velocity in the medium of Teflon spheres and air, we have measured the field transmitted through a sample of Teflon spheres contained in a 7.5 cm diameter copper tube with a length L = 10 cm. In these measurements, the filling fraction of the Teflon spheres is 0.60 which is slightly higher than it is in the metal network. We first determine the index of refraction n for this sample at a frequency ν_0 = 6.45 GHz to be n = 1.26, by measuring the frequency shift of a resonant cavity mode in a medium of Teflon spheres relative to that in air. The absolute phase of the field transmitted through a sample with length L is $\varphi_0 = kL = 2\pi\nu L/v'_{ph}$. Here v'_{ph} is the phase velocity in a copper tube containing the Teflon spheres and is given by $v'_{ph} = v_{ph}[1-(\nu_c^{wg}/\nu)^2]^{-1/2}$ [92], where

$v_{ph} = c/n$ is the phase velocity in an unbounded medium of Teflon spheres and ν_c^{wg} is the cutoff frequency of the cylindrical waveguide. The value of $\nu_c^{wg} = 2.06$ GHz in this case was determined experimentally from measurements of the transmission through the copper tube filled with Teflon spheres from 1 to 4 GHz. Using these relations and the index of refraction measured at ν_0 we determine the absolute phase $\varphi_0 = 2\pi\nu_0 L/v'_{ph}$. Then, starting from this frequency, we measure the frequency dependence of the field transmitted through the sample of Teflon spheres contained in a copper tube. Transmission spectra were obtained for 1000 different sample configurations. The small variation between configurations of less than 1% of the field amplitude indicates that the scattering due to the Teflon spheres is extremely weak. This explains the persistence of the band gap when the network is filled with Teflon spheres. The real part of the ensemble average complex field $<Ecos\varphi>$ is shown in Fig. 29. The well defined sinusoidal frequency dependence of $<Ecos\varphi>$ allows us to follow the phase roll-up with frequency. By following the increase in the phase of the transmitted field when the frequency is changed in small increments of 2.5 MHz, we are able to obtain the phase $\Delta\varphi$ accumulated between 6.45 and 10.0 GHz. By adding the accumulated phase $\Delta\varphi$ to the absolute phase φ_0 we determine the absolute phase in this frequency range. From this phase, we calculate the phase velocity v_{ph} in a medium of Teflon spheres and air contained in a copper tube. The frequency dependence of v_{ph} is shown in Fig. 30. Using Maxwell-Garnet approximation [93], small corrections to v_{ph} are made to determine the phase velocity in the Teflon-air medium within the metal network. At a frequency equal to the

cutoff frequency for the metal structure filled with Teflon spheres, the phase velocity is 2.39×10^{10} cm/s. This gives $v_{ph}/c = 0.80$ which is close to the ratio of the cutoff frequencies of the network in Teflon and in air of 0.81.

When some of the Teflon spheres are replaced by aluminum spheres, transmission peaks appear below the band edge. Measurements have been made for two filling fractions of aluminum spheres $f_{al} = 0.05$ and $f_{al} = 0.10$. A typical transmission spectrum at a filling fraction of the aluminum spheres of 0.05 is shown in Fig. 31. The peaks below the cutoff frequency are reminiscent of modes associated with "donor" defects which have been observed in 3D dielectric PBG materials [58]. However, the radius of the scattering spheres in the present case is at least an order of magnitude smaller than the wavelength. Thus these transmission peaks are more likely associated with random configurations of many metal spheres rather than with individual scatterers.

We characterize the strength of the disorder of the scattering medium at an aluminum filling fraction of 0.10 by measuring the scattering length ℓ_s of the Teflon - aluminum mixture apart from the metal lattice. The scattering length is determined by measuring the intensity associated with the average field $I_{coh} = |< E >|^2$ as a function of the sample length L. In a sample tube with a diameter which is larger than the wavelength in the medium, the coherent intensity falls exponentially with an attenuation length which is close to the scattering length, once the sample is long enough that a single waveguide mode predominates or has a large enough diameter so that the incident wave can couple effectively to a large number of modes with

small components of transverse momentum. In this case, $I_{coh} \sim I_0 exp(-L/\ell_s)$. The average field for 2000 sample configurations in the frequency range from 4 to 10 GHz was obtained for various thicknesses. By averaging over an ensemble of samples, the diffusive component of the field tends towards its average value of zero. From measurements with sample length from 7.5 to 25 cm we find that $\ell_s \geq 20$cm at 4 GHz and that it decreases to $\ell_s = 4.5 \pm 0.5$ cm at 10 GHz. Since $\ell_s \geq \ell$. where ℓ is the transport mean free path, the measurements show that $k\ell$ is greater than 10 over the entire frequency range. Since localization in samples without long-range order is expected when $k\ell \sim 1$ this indicates that microwave radiation in the mixtures of Teflon and aluminum spheres apart from the metal network is far from the localization threshold. The values of k used in the estimate are calculated using the phase velocity in a random medium of Teflon spheres.

In Fig. 32, we present the average transmission spectra for 200 sample configurations for the two concentrations of aluminum spheres. In these measurements, different sample configurations were created shaking the sample by hand. In the average spectrum the band edge is broadened relative to that of the metal network in air and with Teflon spheres inside. The band gap becomes less pronounced as the density of metal scatterers increases. The frequency of the peak in the transmission at low frequencies, however, is not affected. This indicates that the phase velocity is not changed substantially by the insertion of metal spheres into the network. The fluctuations in the phase velocity due to the presence of metal scatterers does not, therefore, appear to cause a smearing of the band edge.

We recall that $var(s_{ab})$ was found to be a reliable measure of the approach to localization. We investigate the behavior of the second moment, $<s_{ab}>= var(s_{ab}) + 1$, of the intensity transmitted through the structure filled with mixtures of Teflon-aluminum spheres as the frequency is tuned through the band gap edge. A sharp increase is observed with a maximum value of approximately 4.5 which indicates localization transition.

6.4 Conclusions

In conclusion, we have observed a band of attenuated microwave transmission through a 3D periodic metal network. We have shown that filling the metallic network with dielectric scatterers, which are small compared to the electromagnetic wavelength, shifts the band edge to a value proportional to the phase velocity in the medium. This demonstrates that a well defined band gap can be produced in a structure which deviates from perfect periodicity and suggests that useful photonic devices can be produced using structures which are not perfectly periodic. The extent of disorder that can be introduced before the band gap is significantly altered can be studied by introducing a variety of defects into the periodic lattice. In this study, we have measured transmission through a periodic metal wire structure with various concentrations of randomly positioned metallic spheres. We observe a broadening of the band edge which is associated with the presence of localized states in the gap. Because the systems studied are small, the transmission peaks observed may not be associated with sharply defined localized states which can be seen in larger structures. Studies in larger systems would make it possible to investigate the

localization transition in this system. For such samples the ability to observe sharp transmission peaks associated with individual localized modes would be limited by the absorption of the sample.

Summary

In a series of independent microwave experiments, we study the statistics of intensity and total transmission in mesoscopic systems in the approach to localization.

In measurements using long waveguides with volume disorder, we were able to reach the localization threshold. This is the realization using classical waves of the Thouless idea of localization of electrons in long wires. We find that, near the localization length, the probability distributions of intensity and total transmission deviate significantly from negative exponential statistics and from a normal distribution, respectively. For large values of these quantities, the corresponding distribution decay instead as a negative stretched exponential to the power 1/2 and as a simple negative exponential.

We confirm experimentally the relationships between the moments of intensity and total transmission and their full distributions derived from RMT calculations for samples with quasi-1D geometry. These relations unify the statistical description of local and spatially averaged transmittance quantities.

The results of these measurements show that the distributions of intensity and total transmission are not significantly affected even by the presence of strong absorption. In contrast, the ensemble average value of the transmission falls exponentially as a result of absorption. The presence of absorption only postpones somewhat the approach to localization, but does not destroy localization. We find that the

variances of intensity and total transmission are directly related to the degree of nonlocal intensity correlation and serve as a reliable measure of the approach to localization.

We have obtained the auto- and cross-correlation function with frequency shift of the total transmission. These functions are dominated by the long- and infinite-range correlation terms of the intensity correlation function and allow us to experimentally determine the frequency dependence of the infinite-range correlation term for the first time.

In a proof of principle experiment of microwave transmission in a 3D periodic metal wire network possessing a photonic band gap, we demonstrate that, by creating an ensemble of random scatterer configurations within the "photonic crystal". it is possible to investigate the statistics of the localization transition.

In conclusion, in this thesis we have established the nature of intensity and total transmission statistics and show how these can be used to study the localization transition.

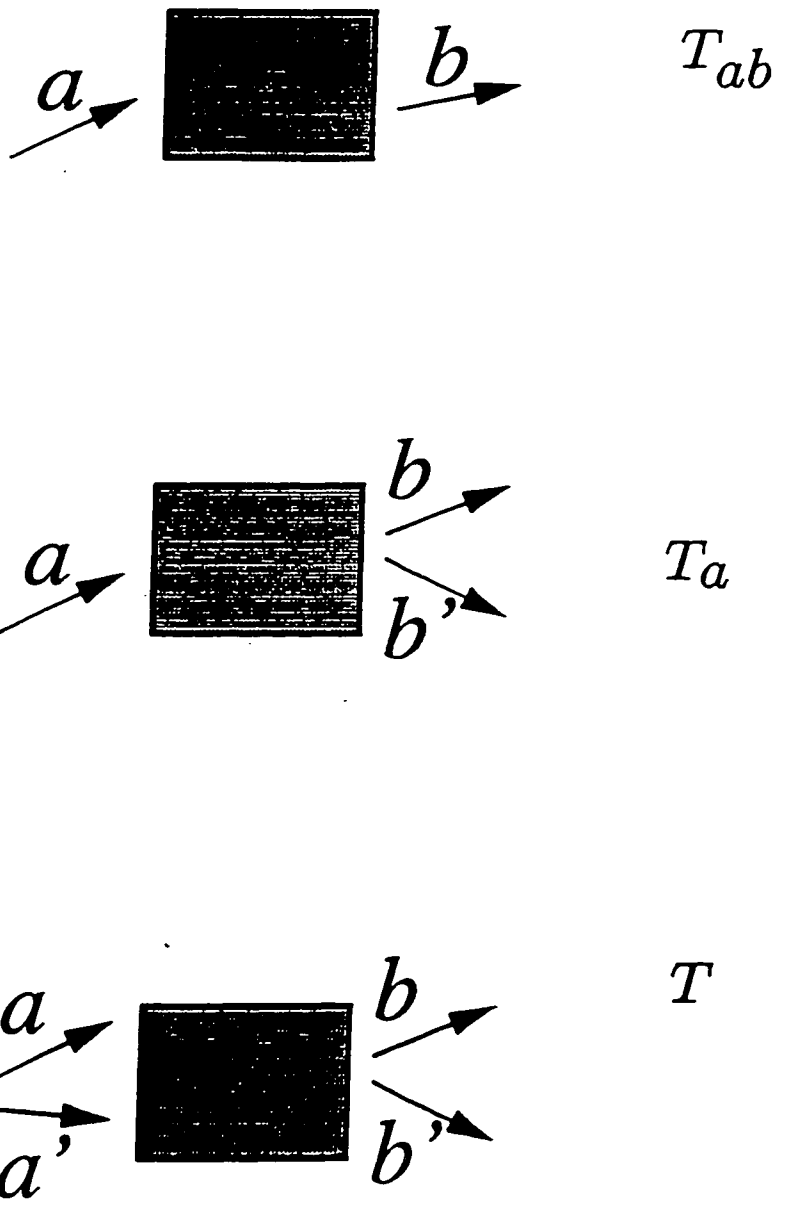

Fig. 1

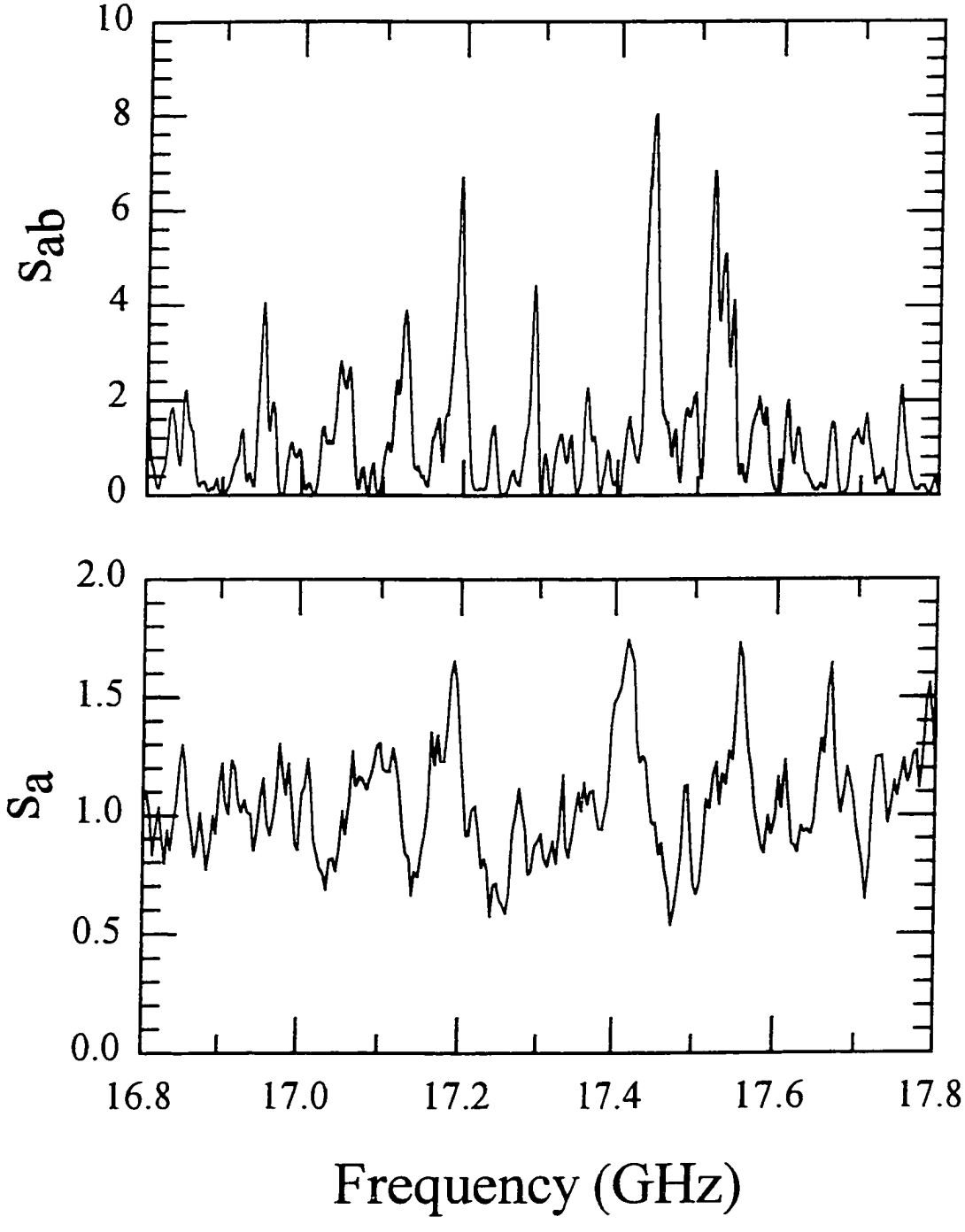

Fig. 2

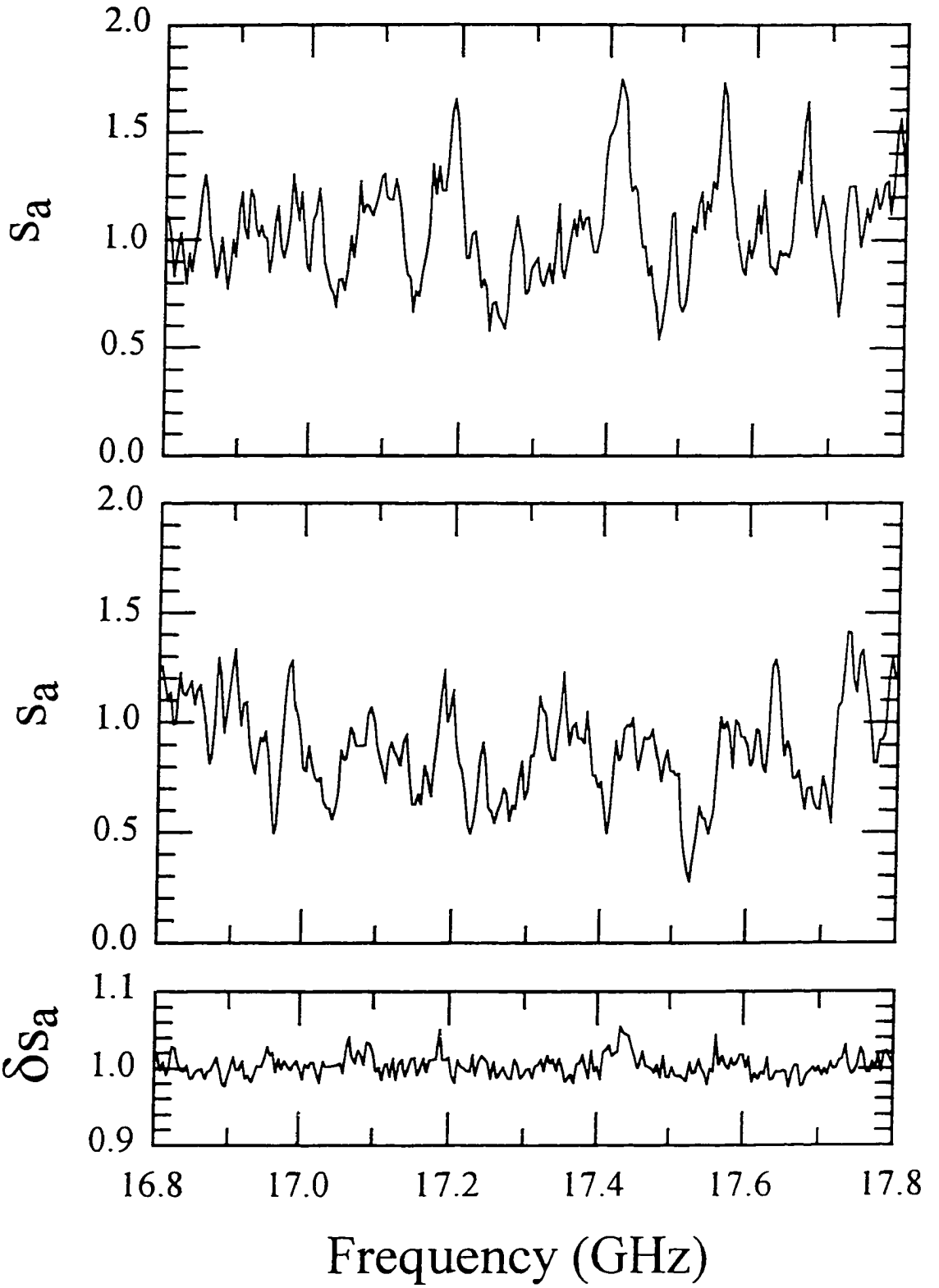

Fig. 3

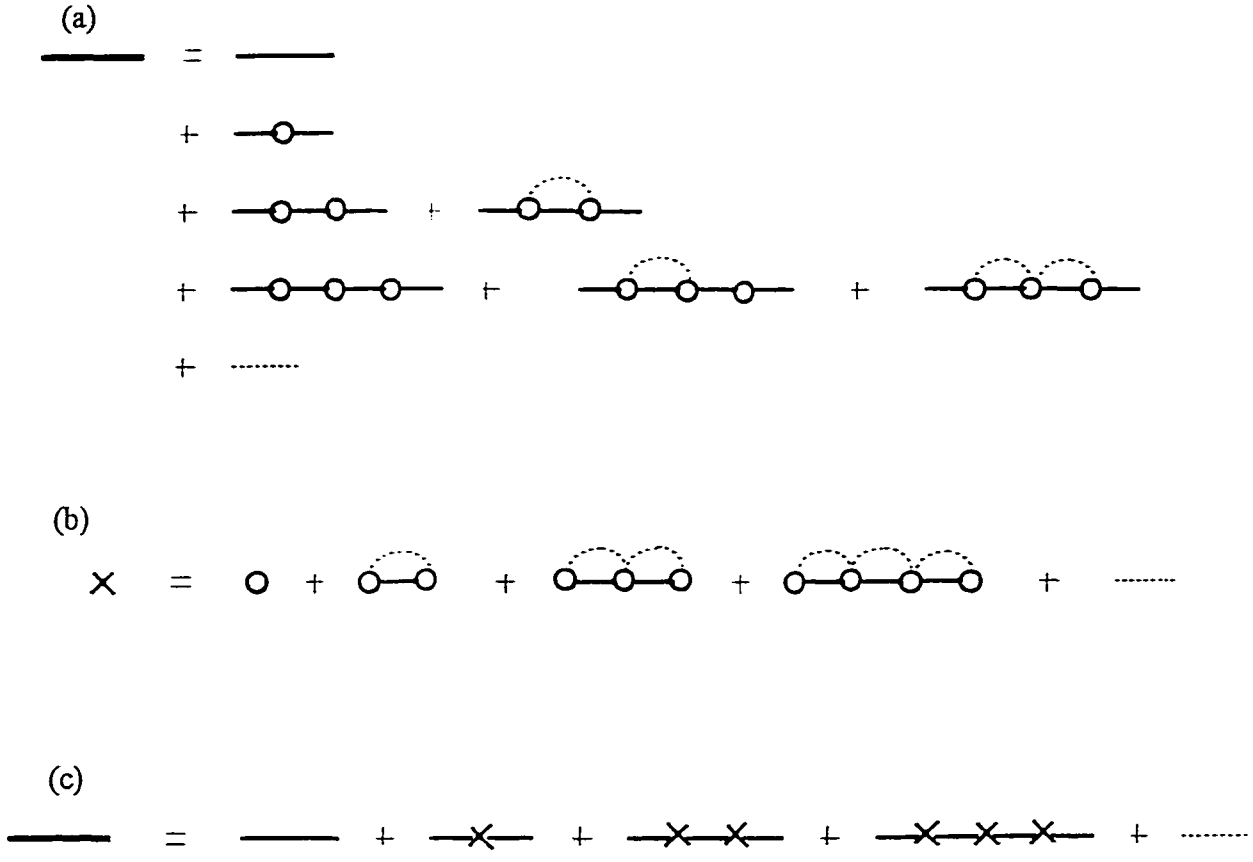

Fig. 4

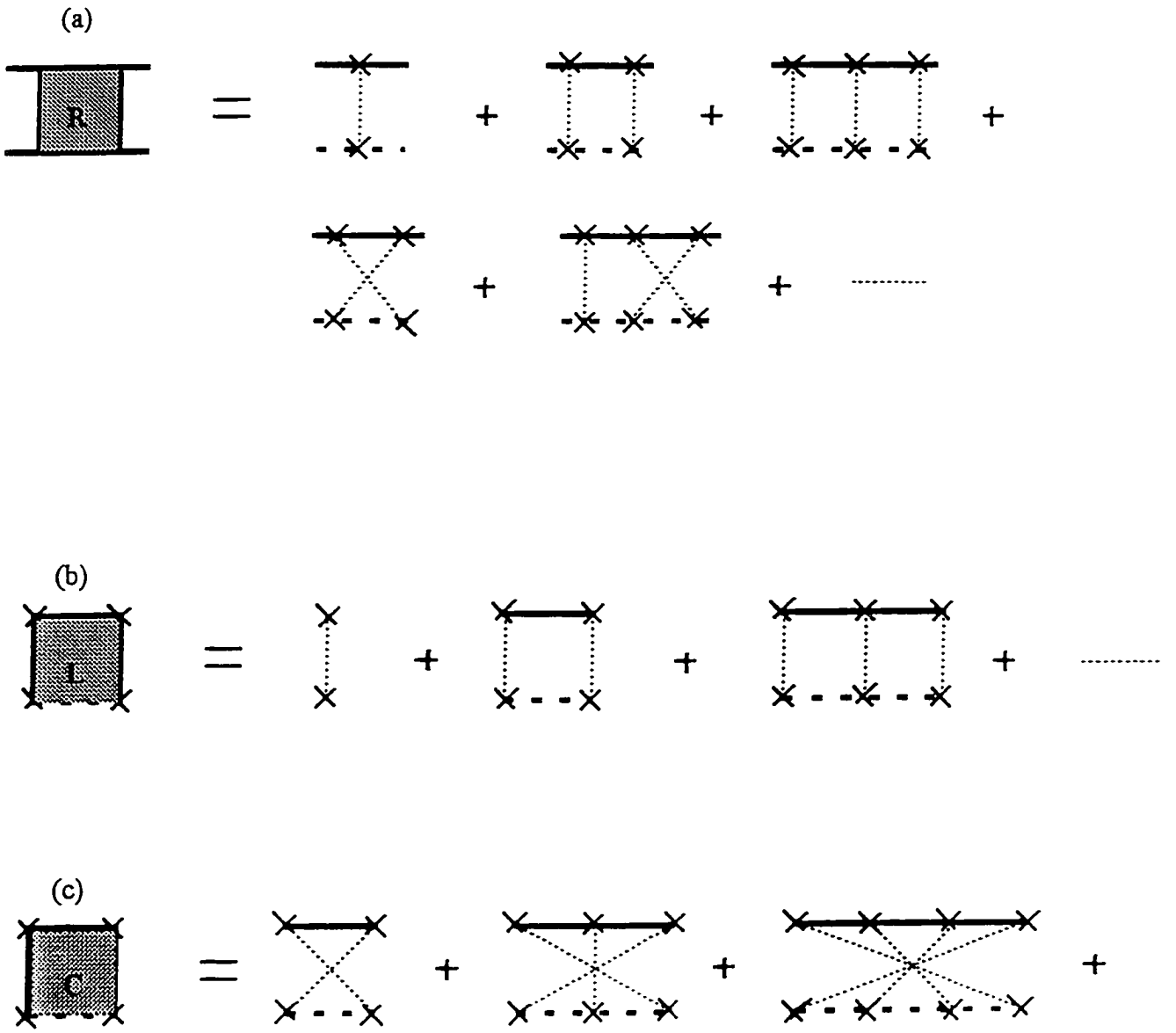

Fig. 5

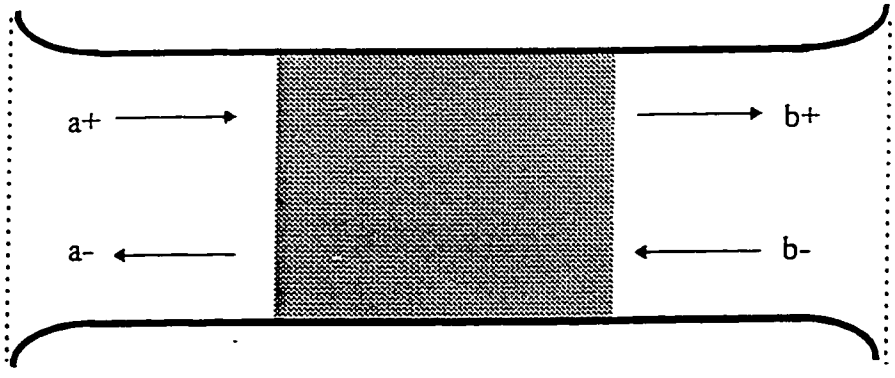

Fig. 6

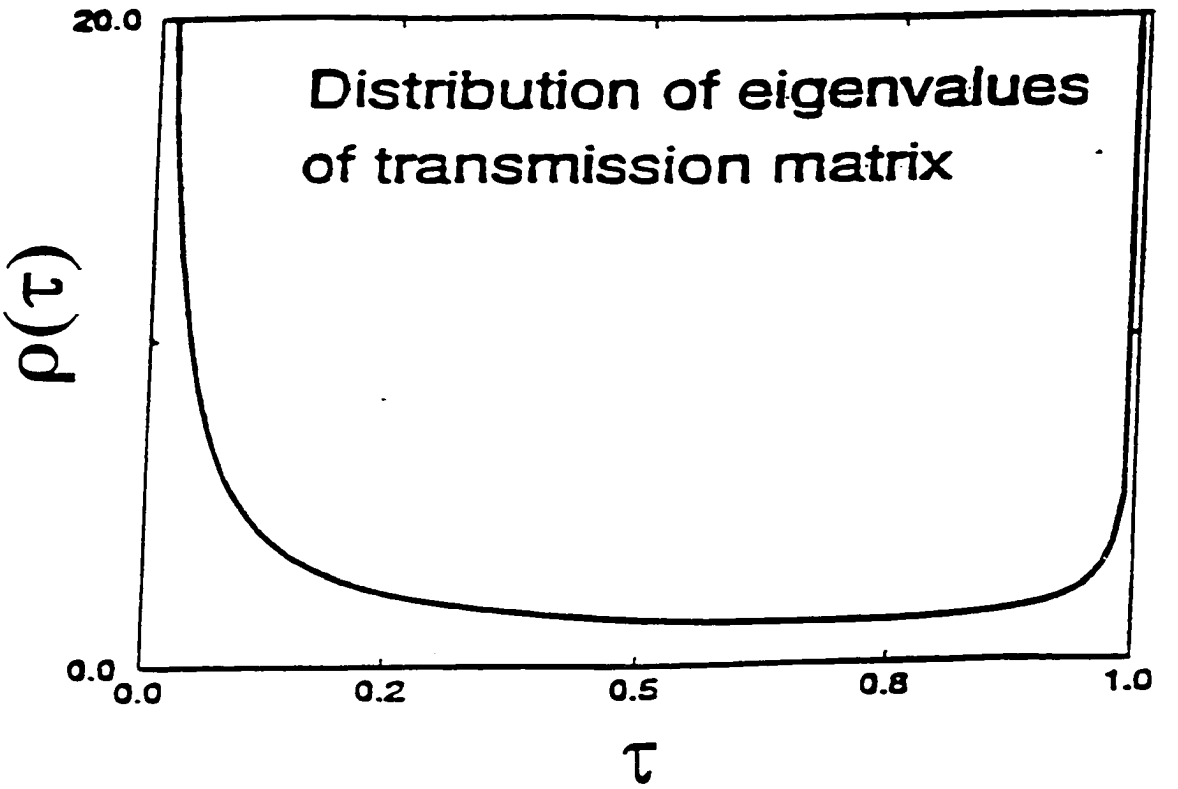

Fig. 7

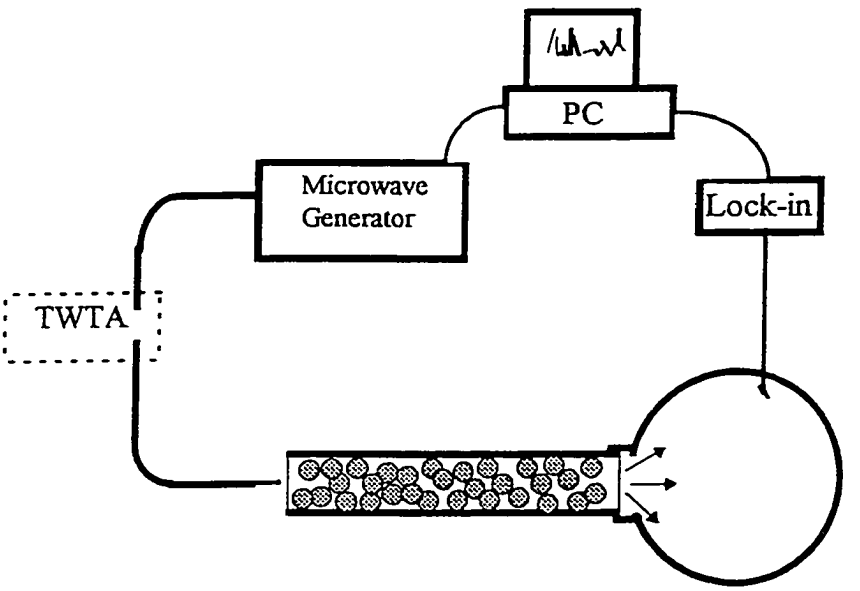

Fig. 8

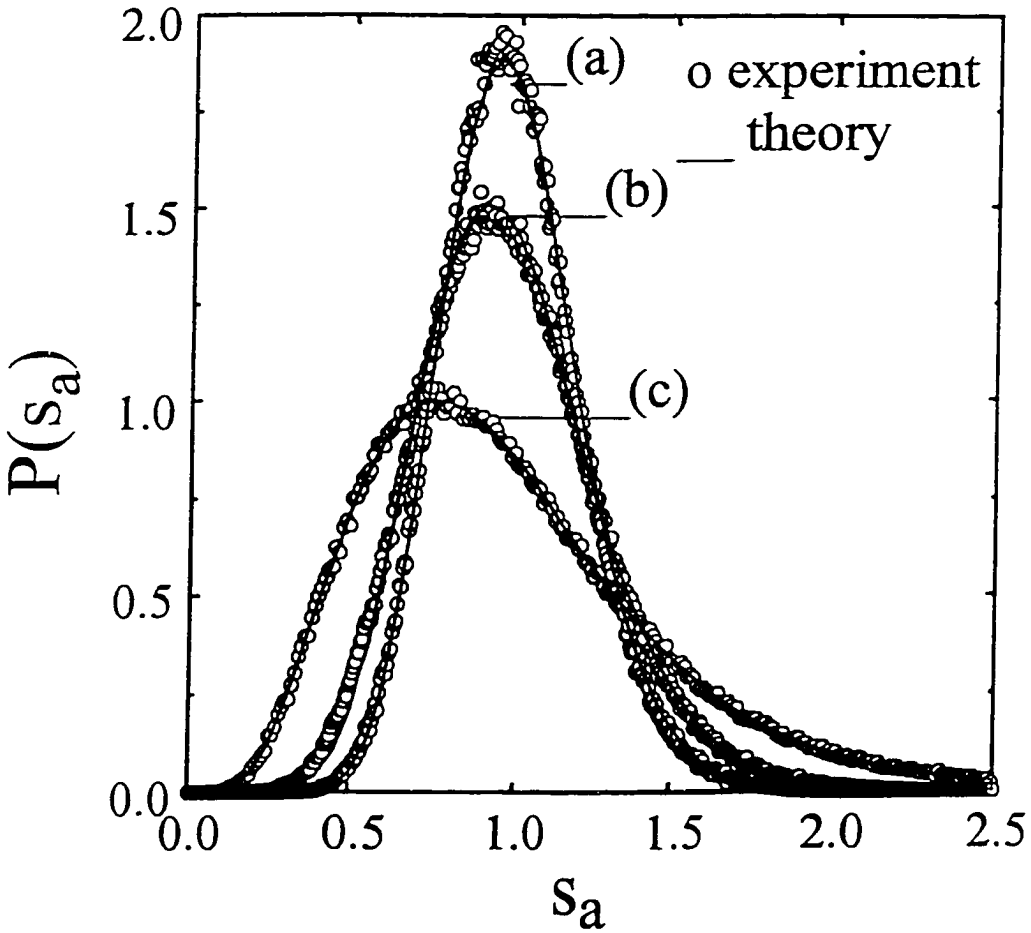

Fig. 9

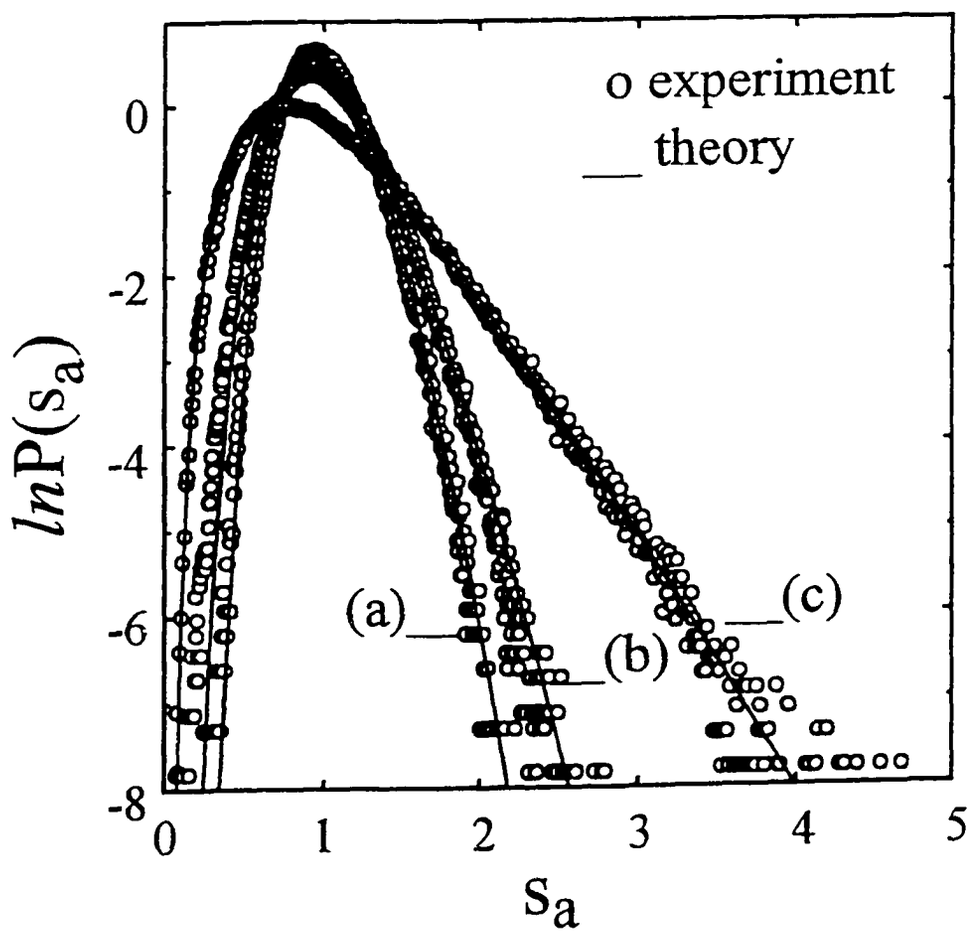

Fig. 10

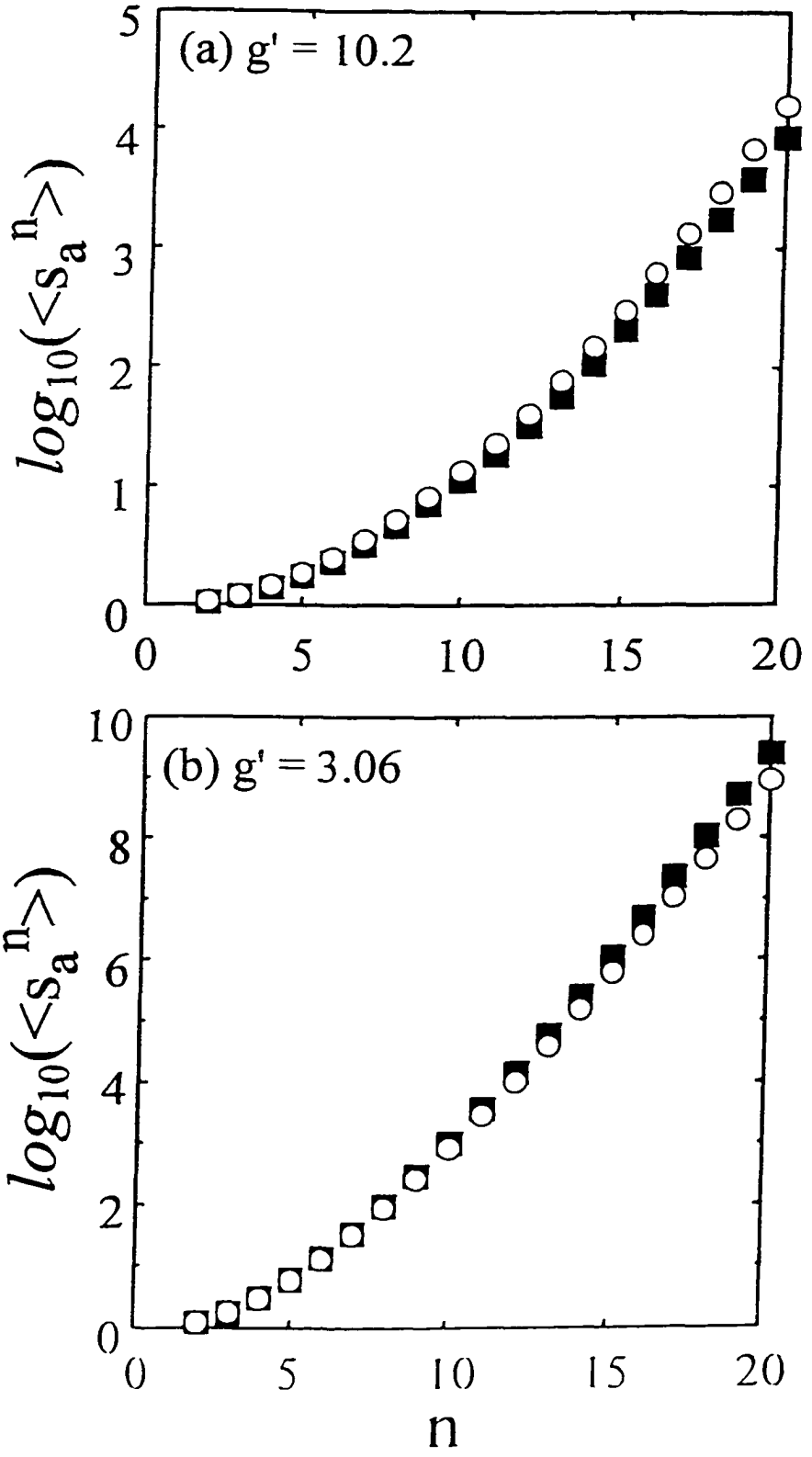

Fig. 11

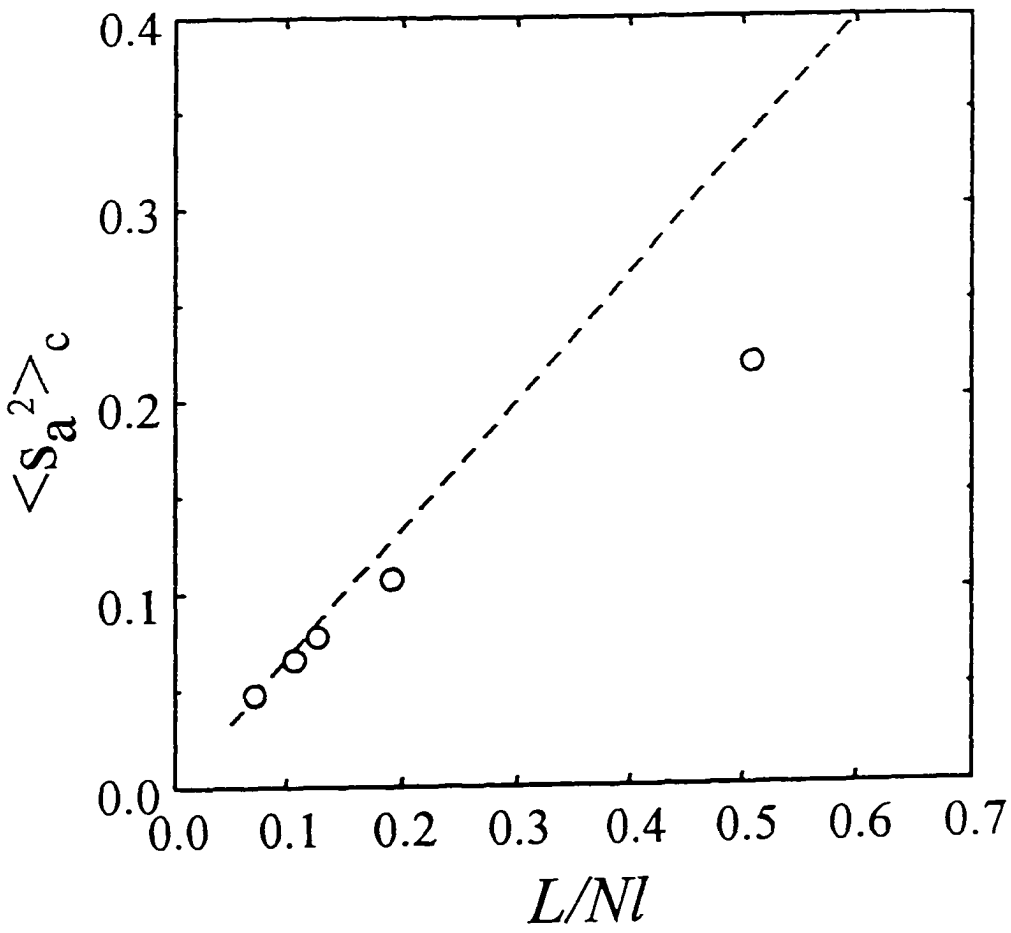

Fig. 12

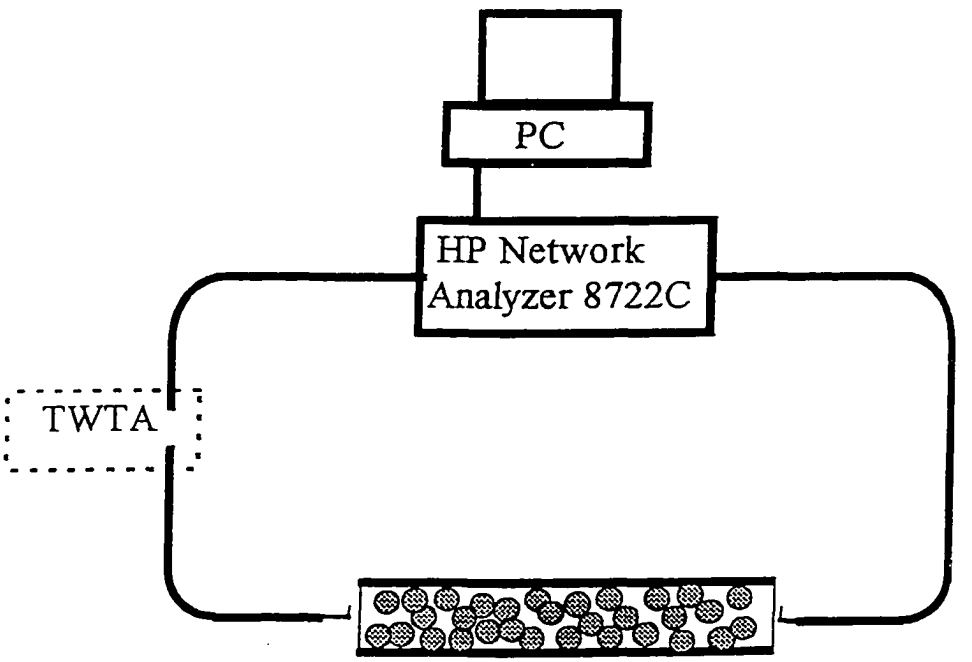

Fig. 13

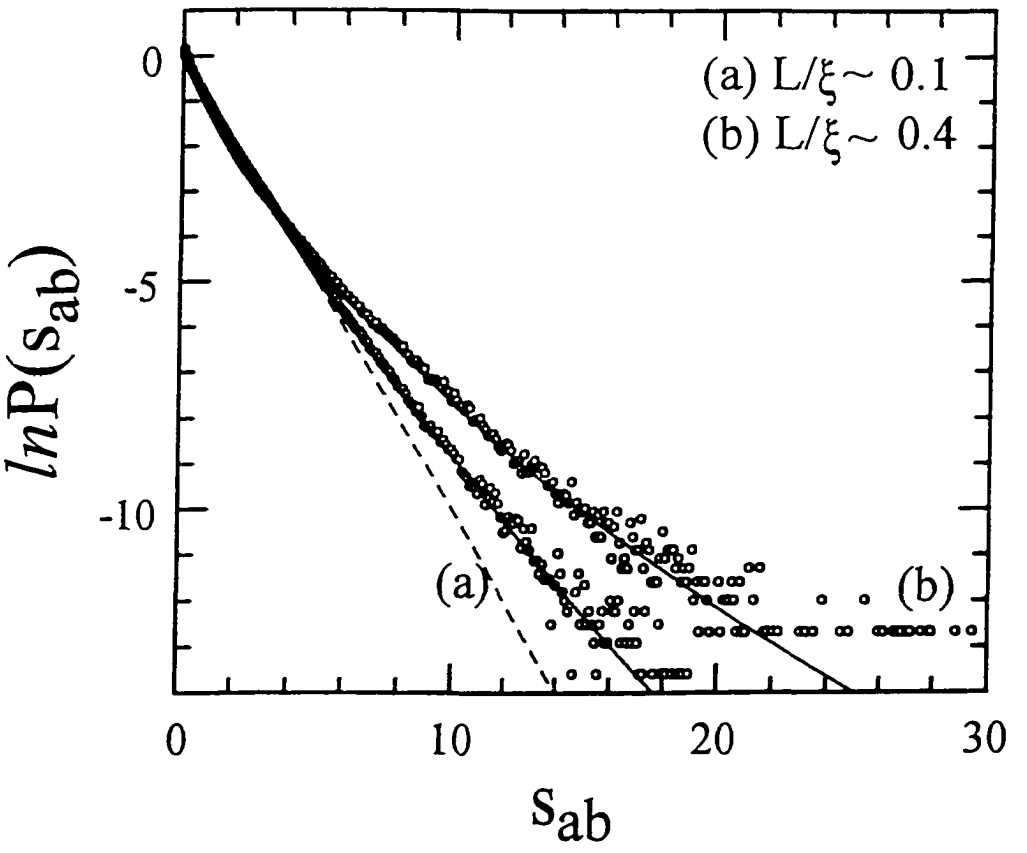

Fig. 14

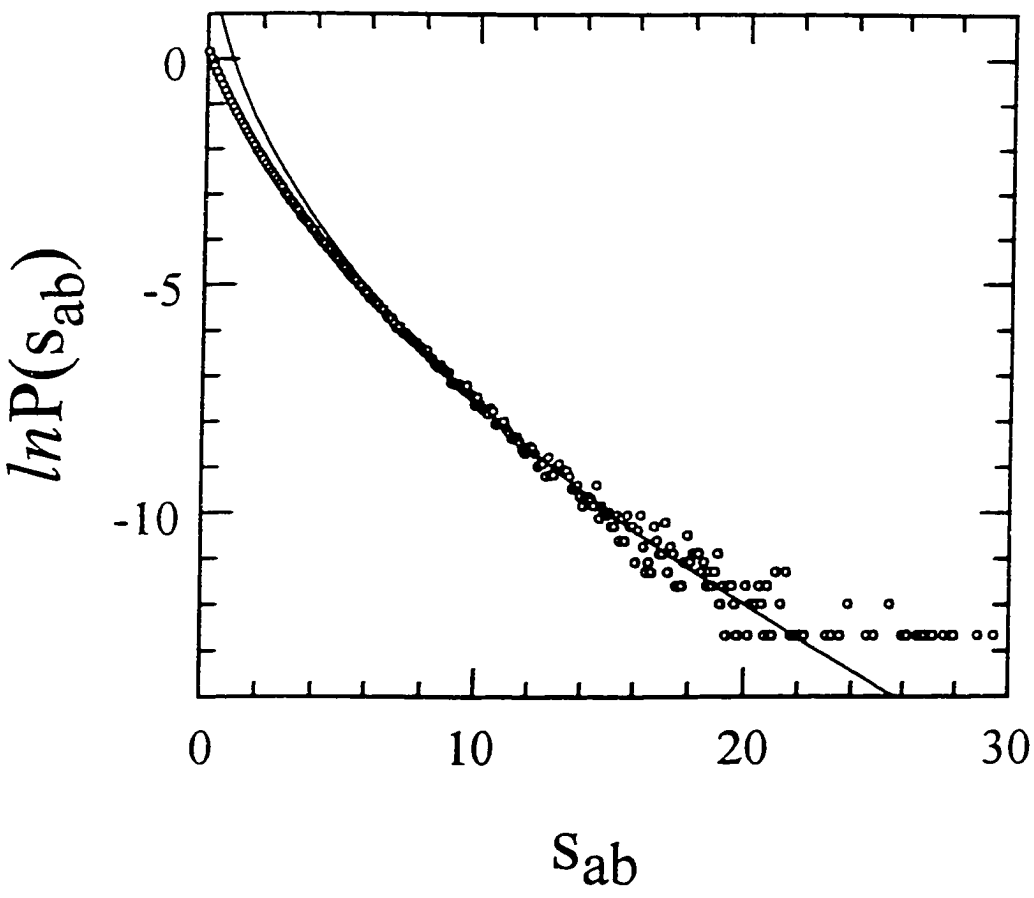

Fig. 15

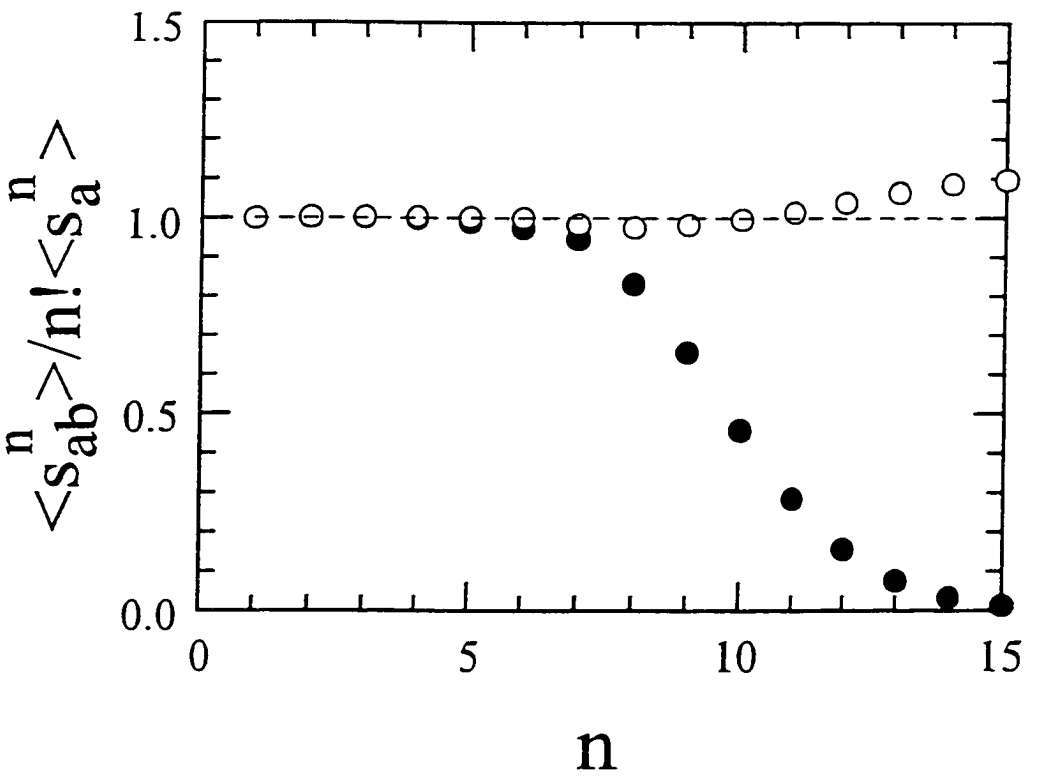

Fig. 16

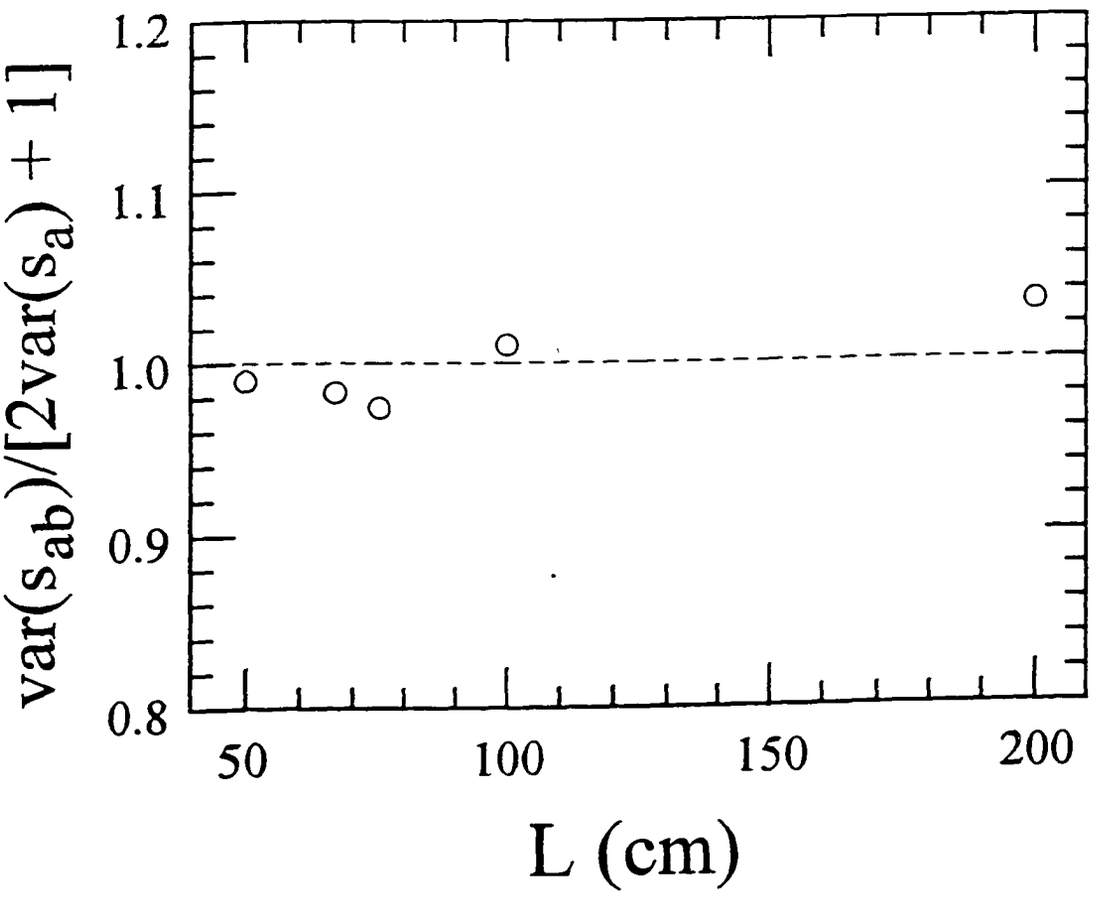

Fig. 17

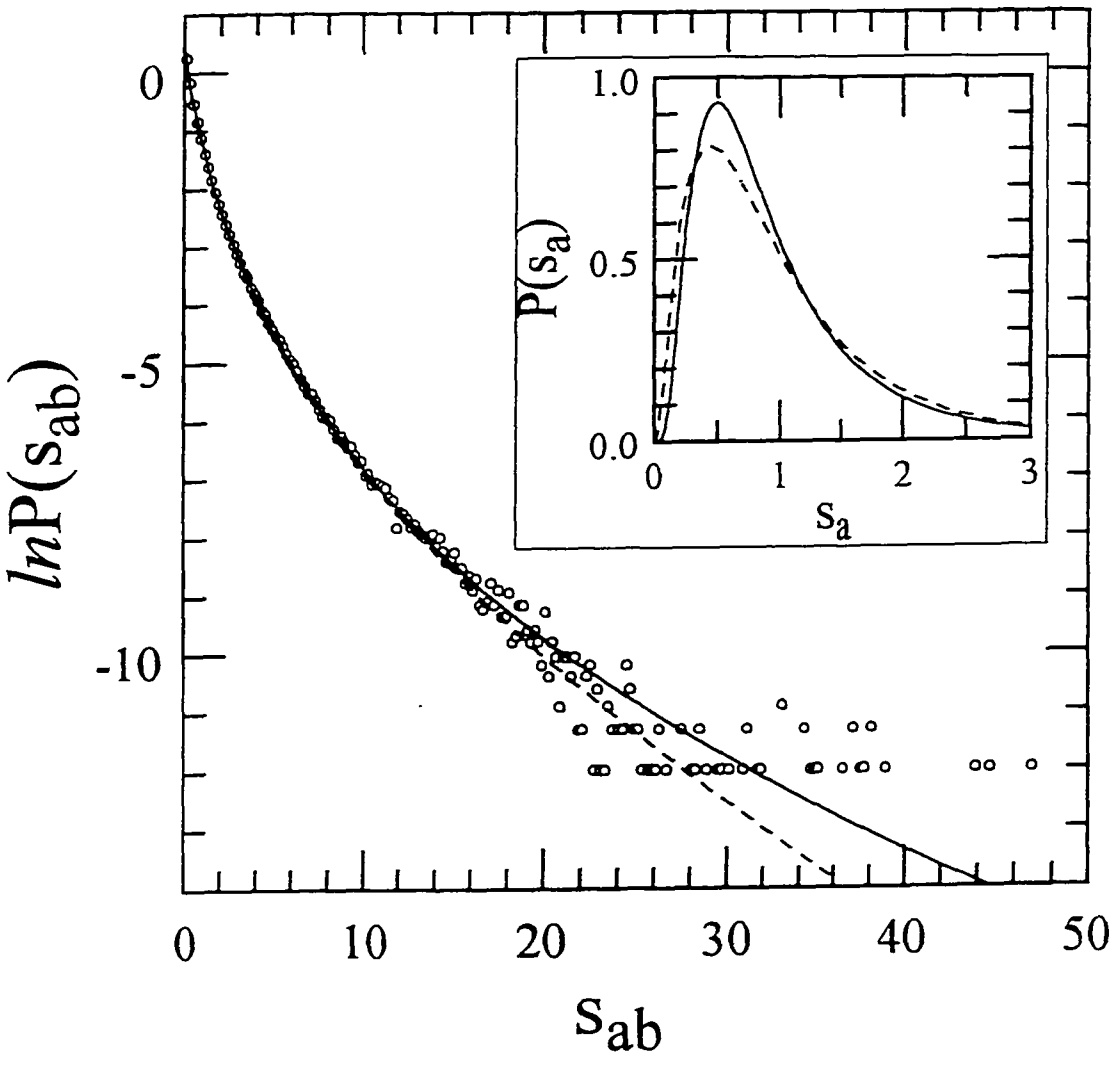

Fig. 18

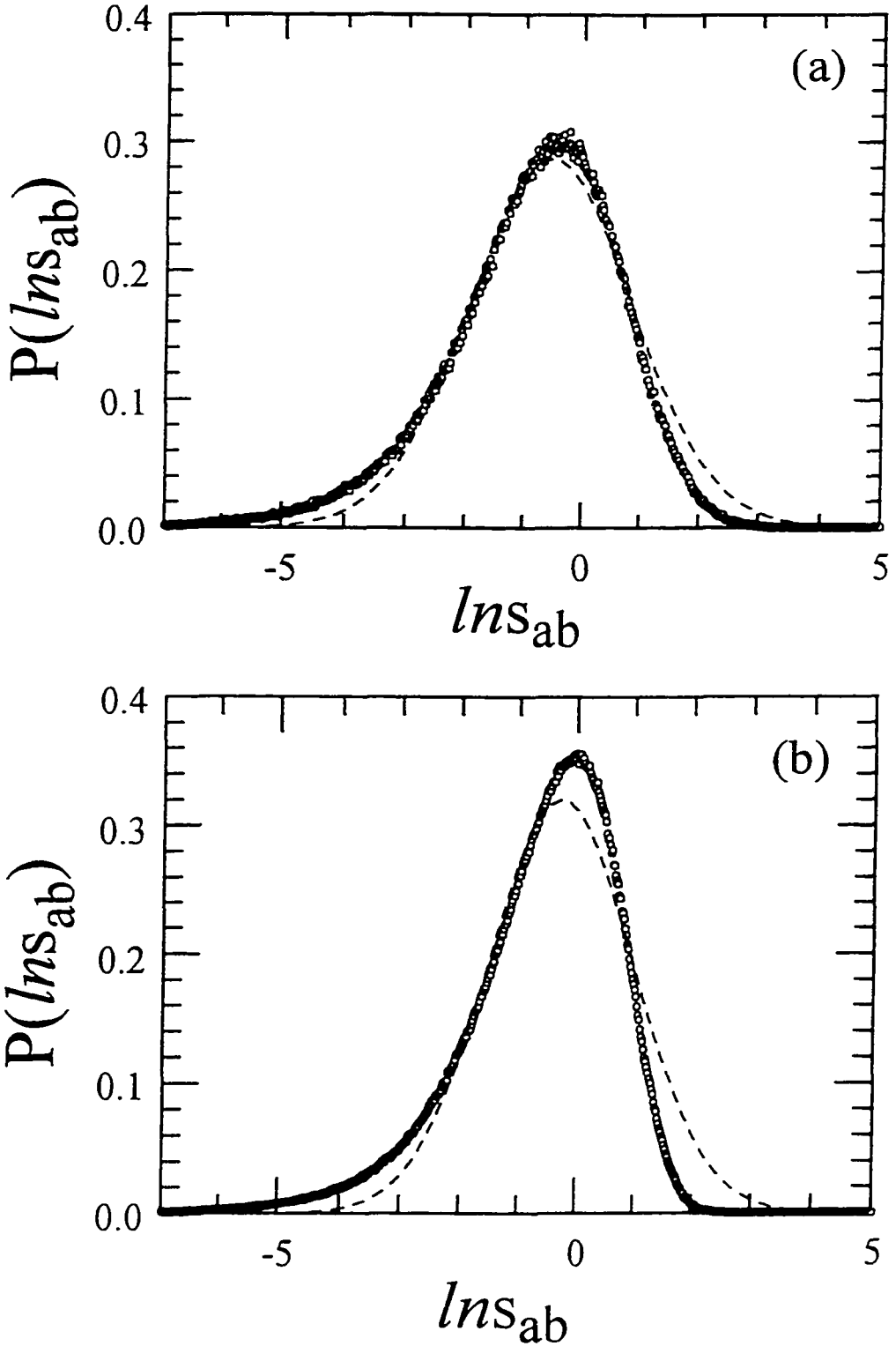

Fig. 19

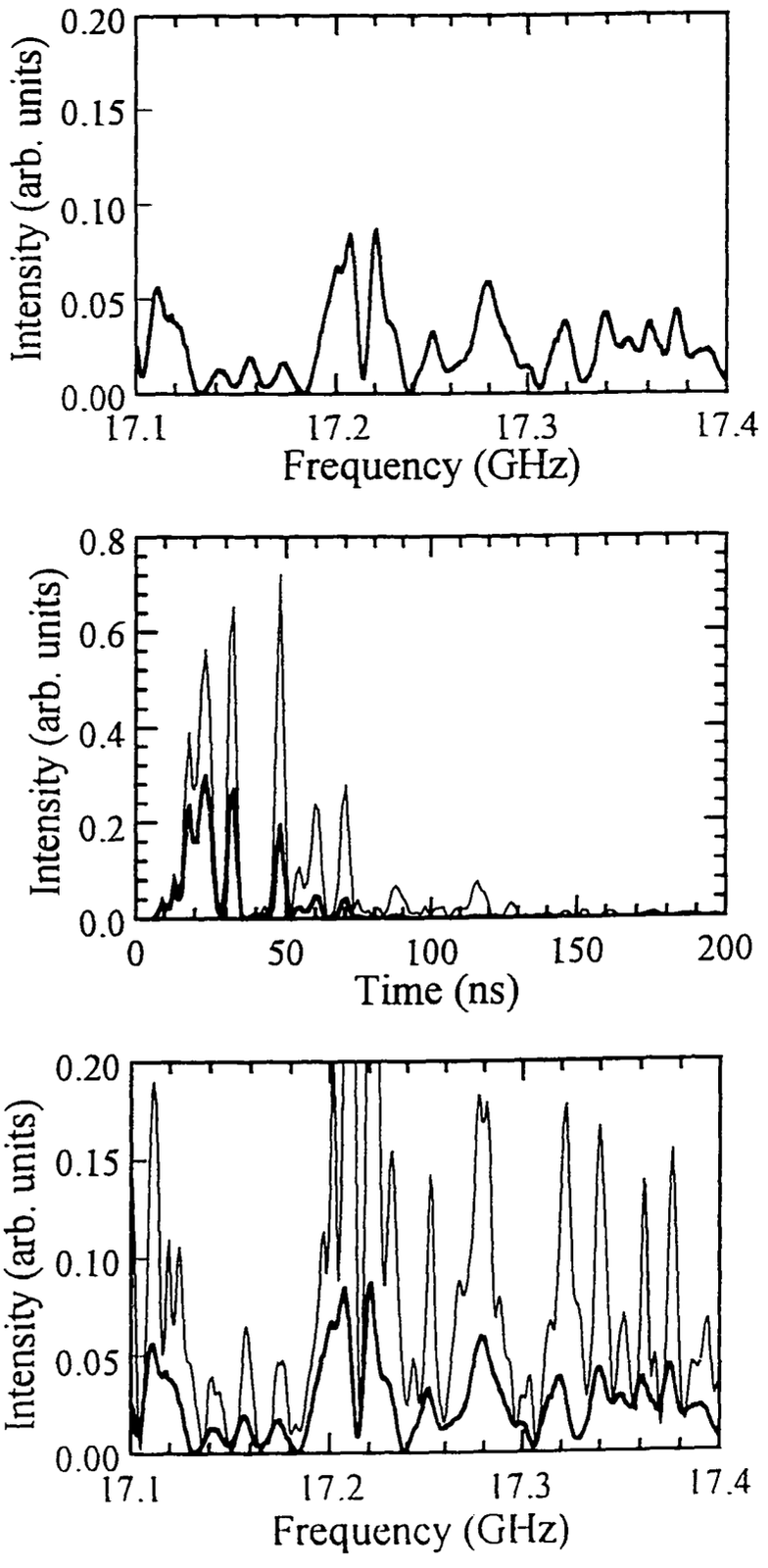

Fig. 20

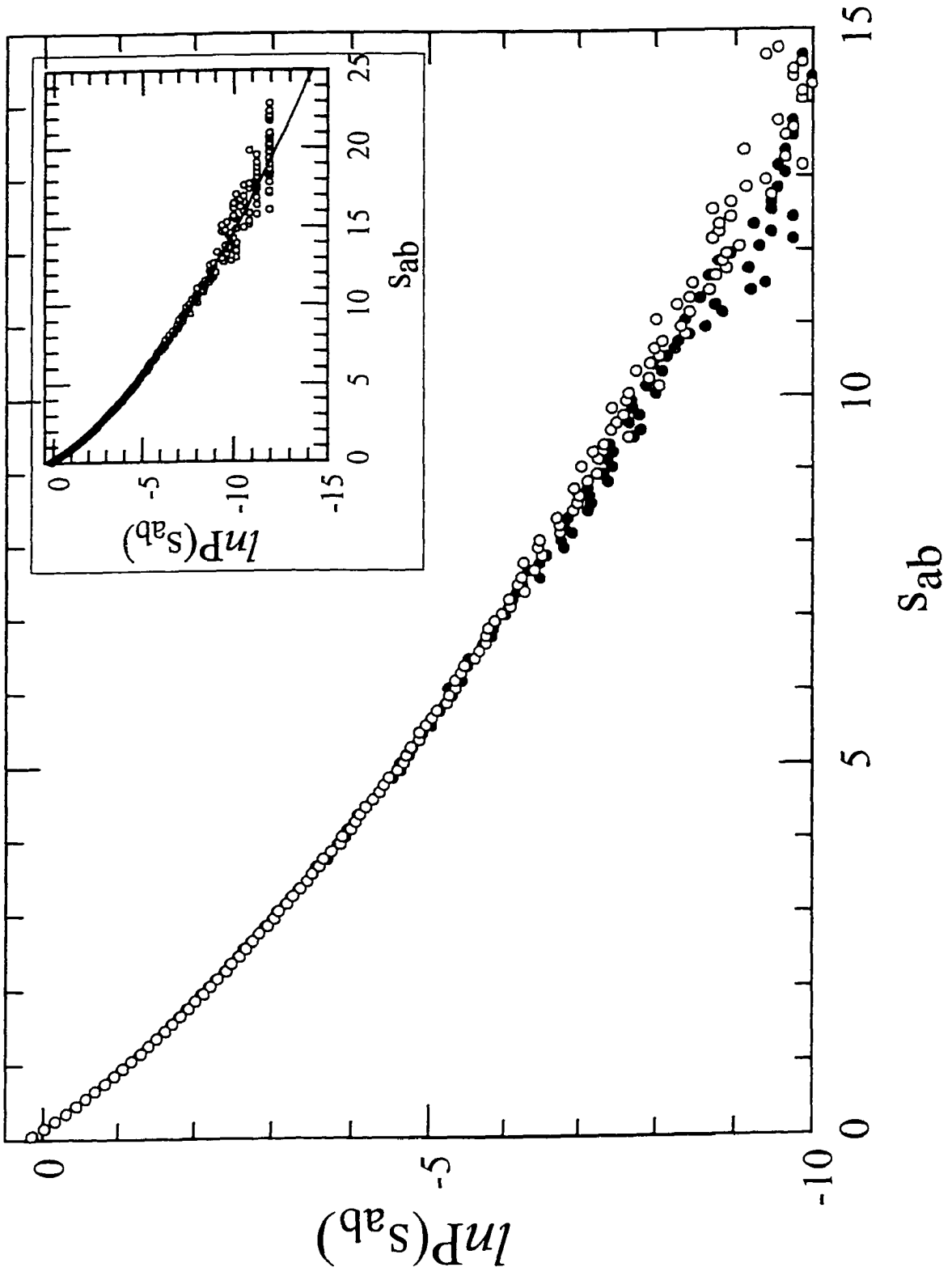

Fig. 21

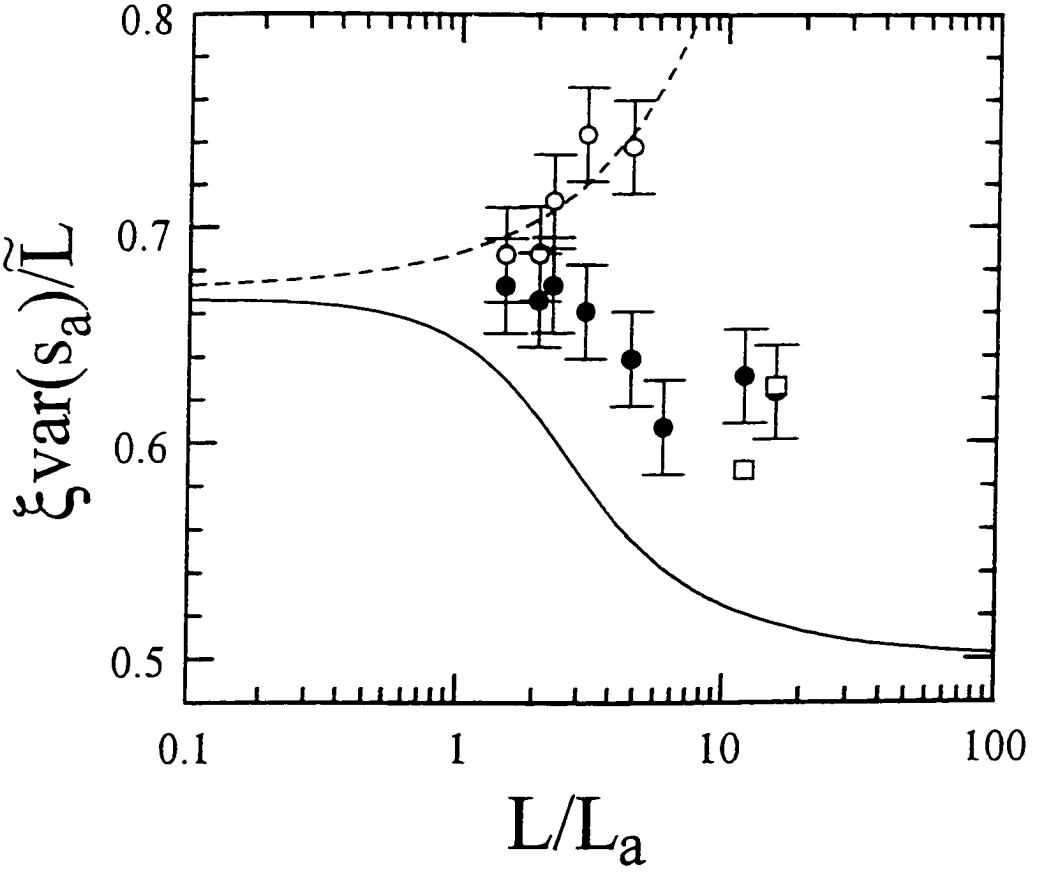

Fig. 22

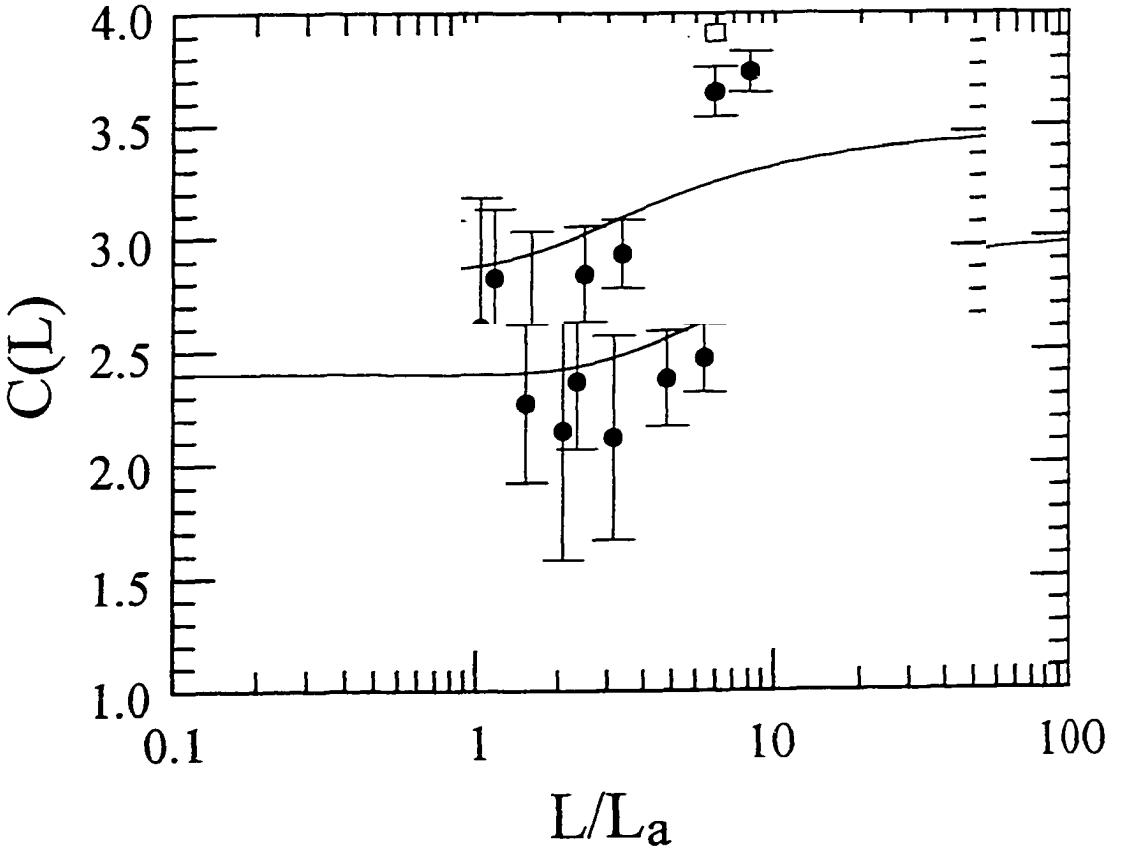

Fig. 23

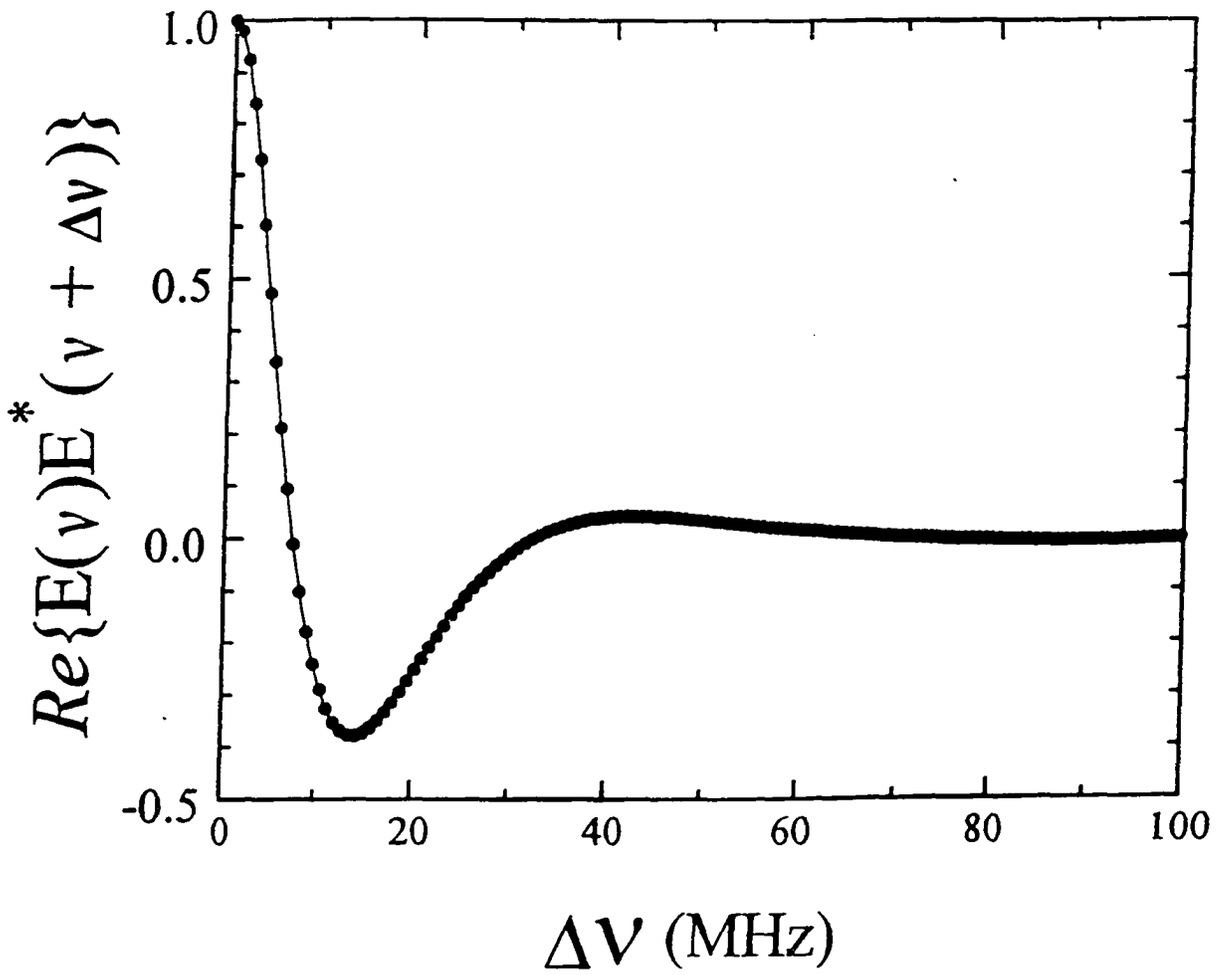

Fig. 24

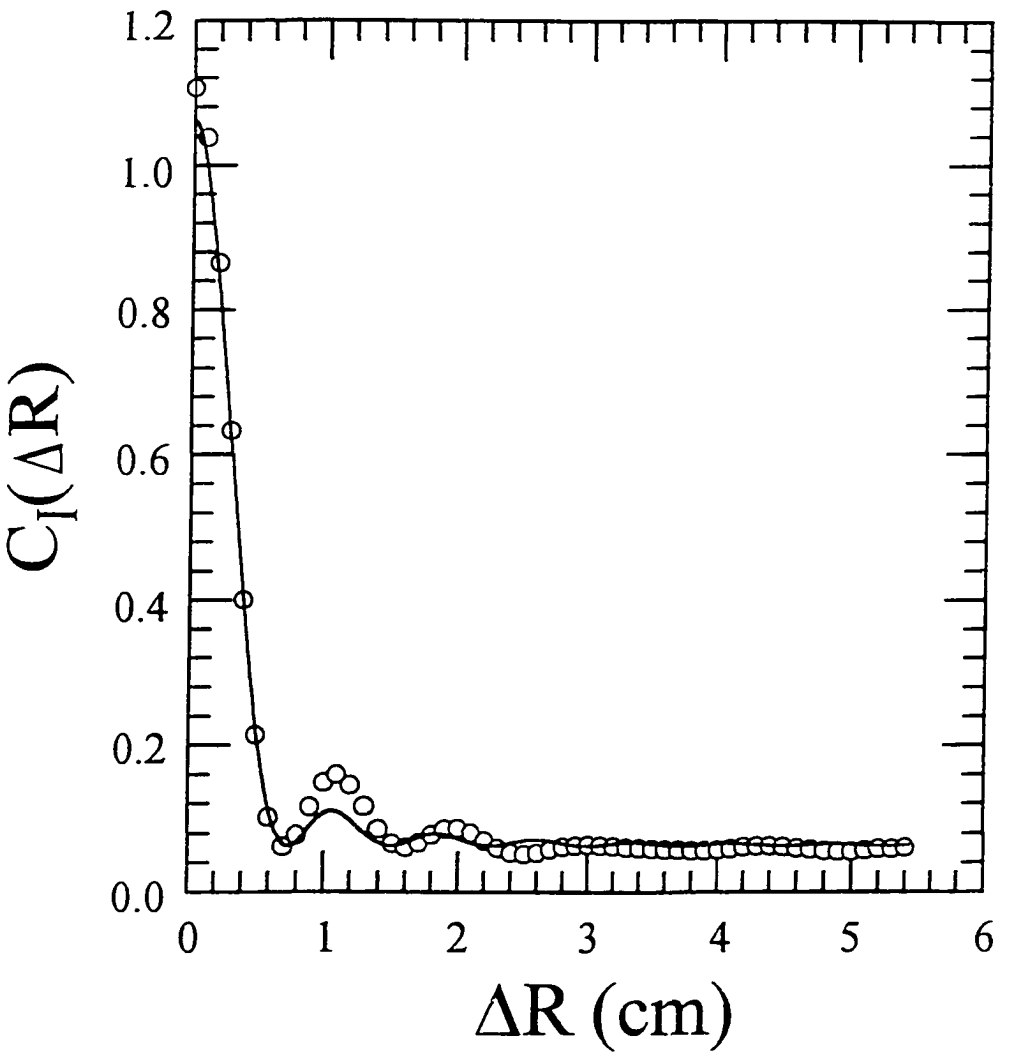

Fig. 25

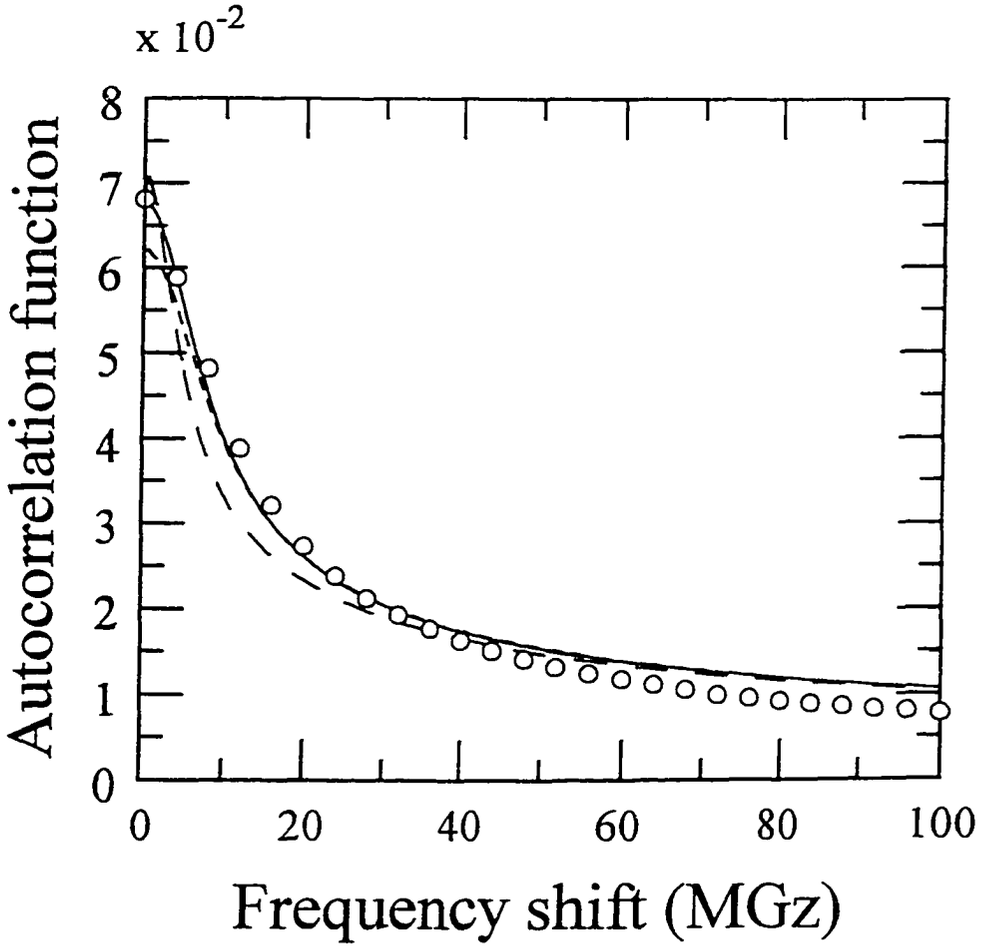

Fig. 26

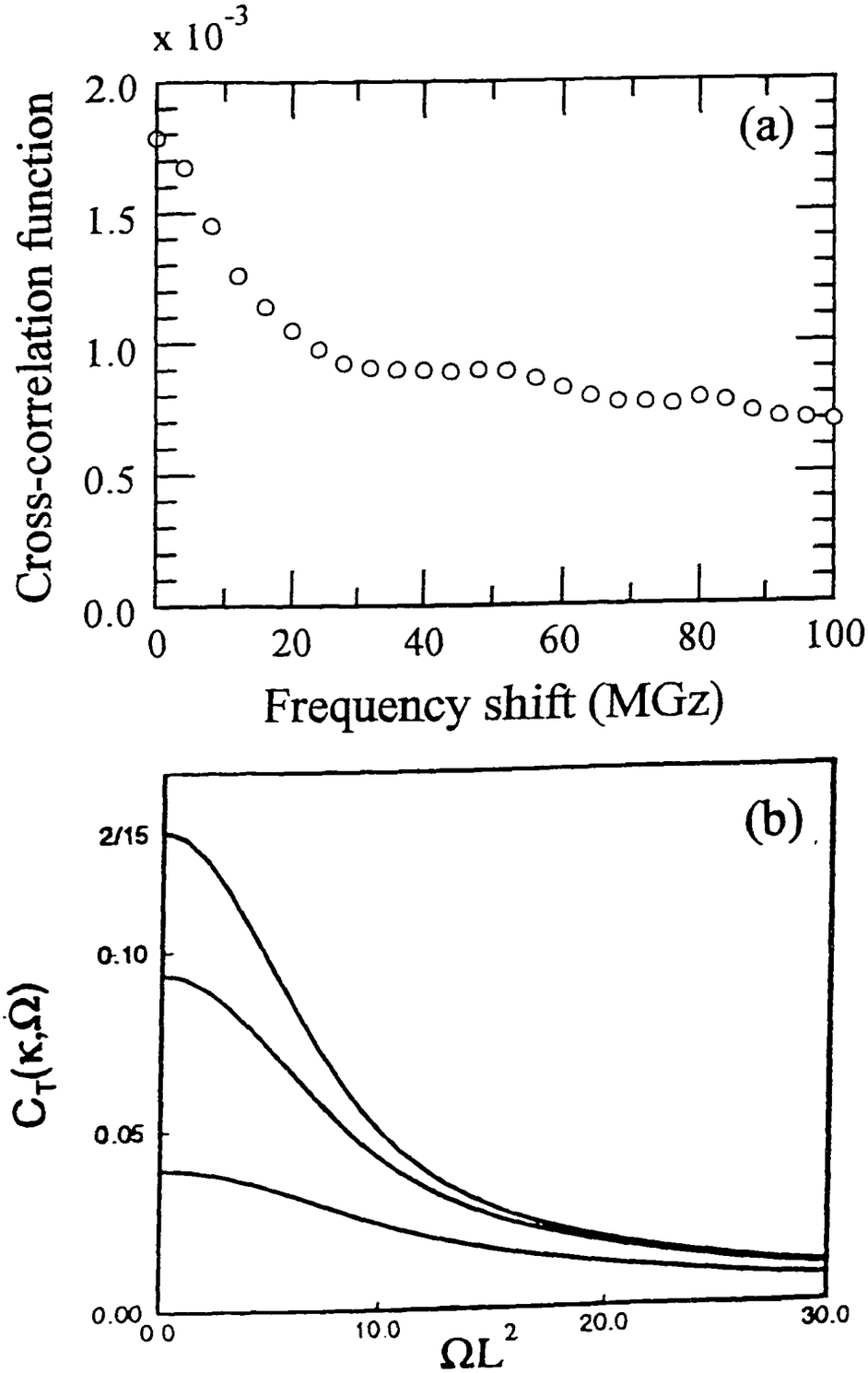

Fig. 27

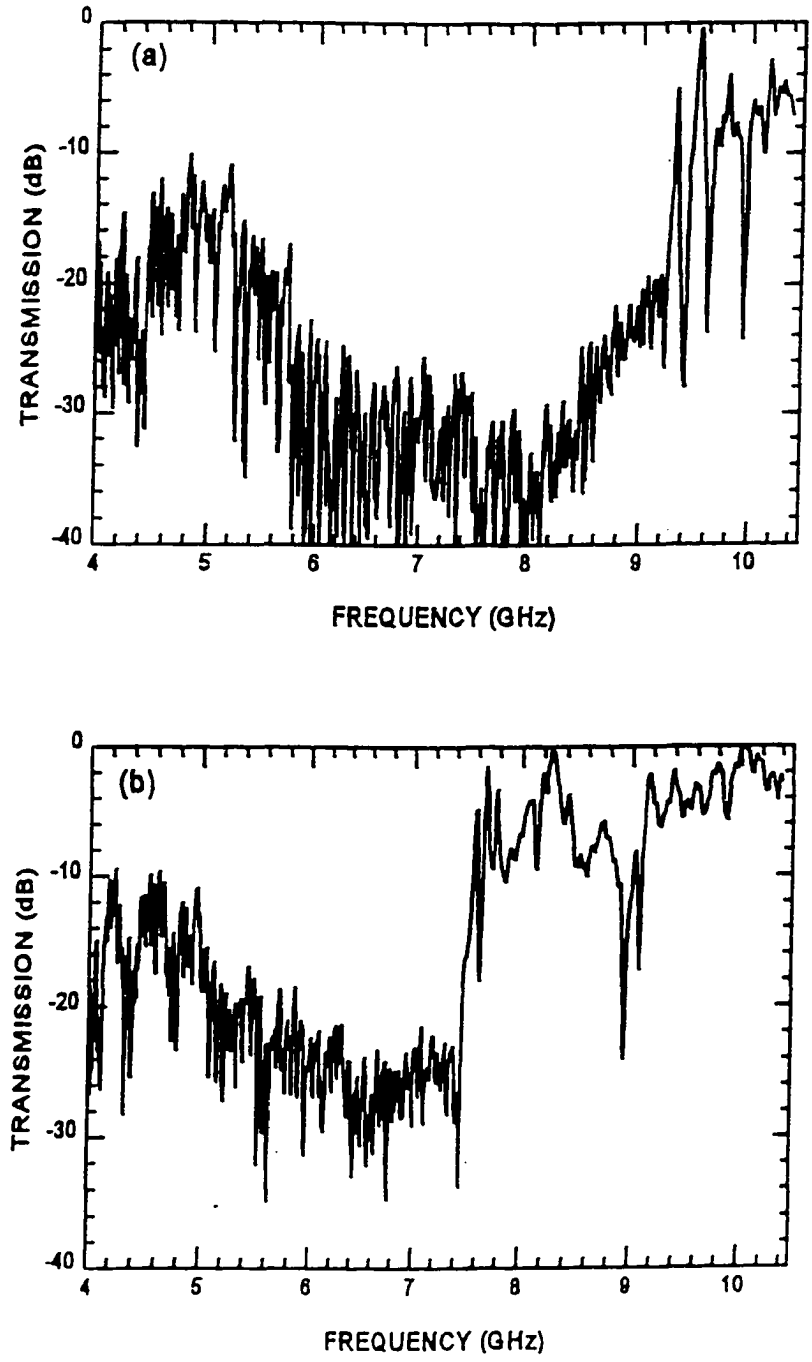

Fig. 28

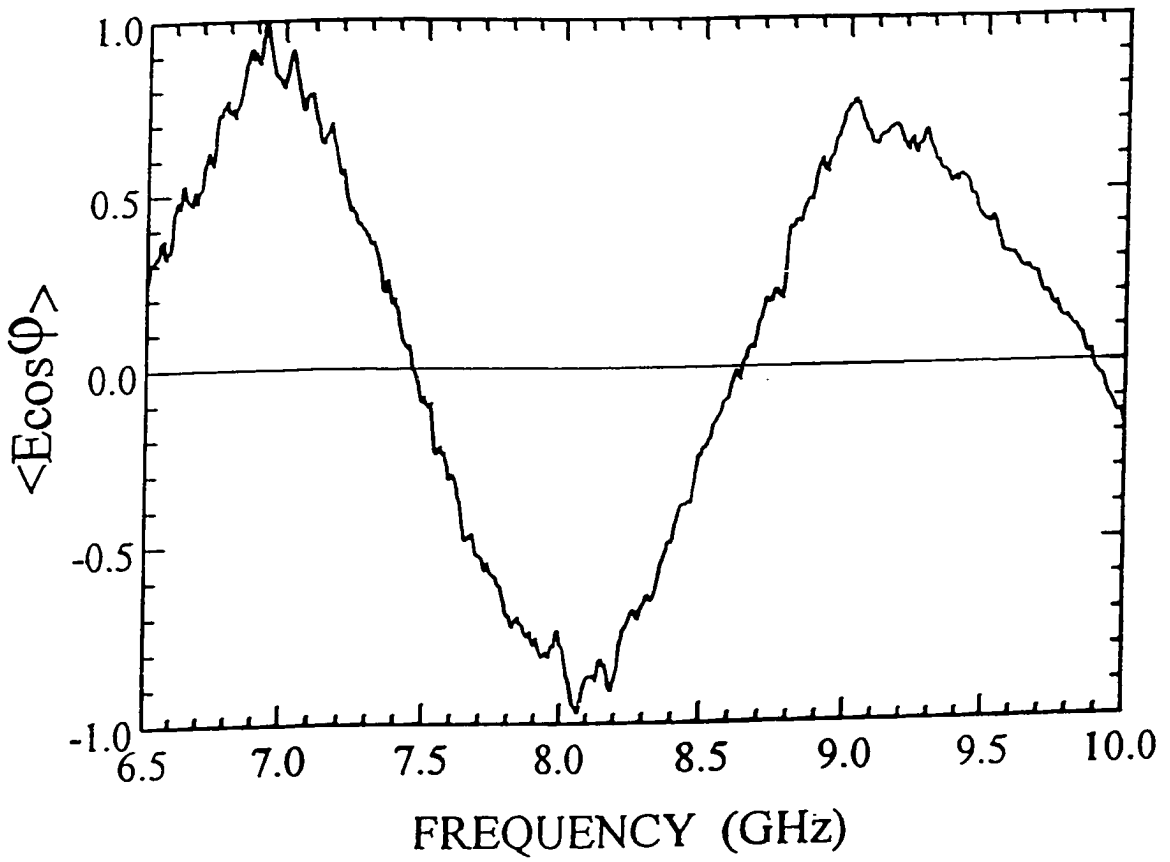

Fig. 29

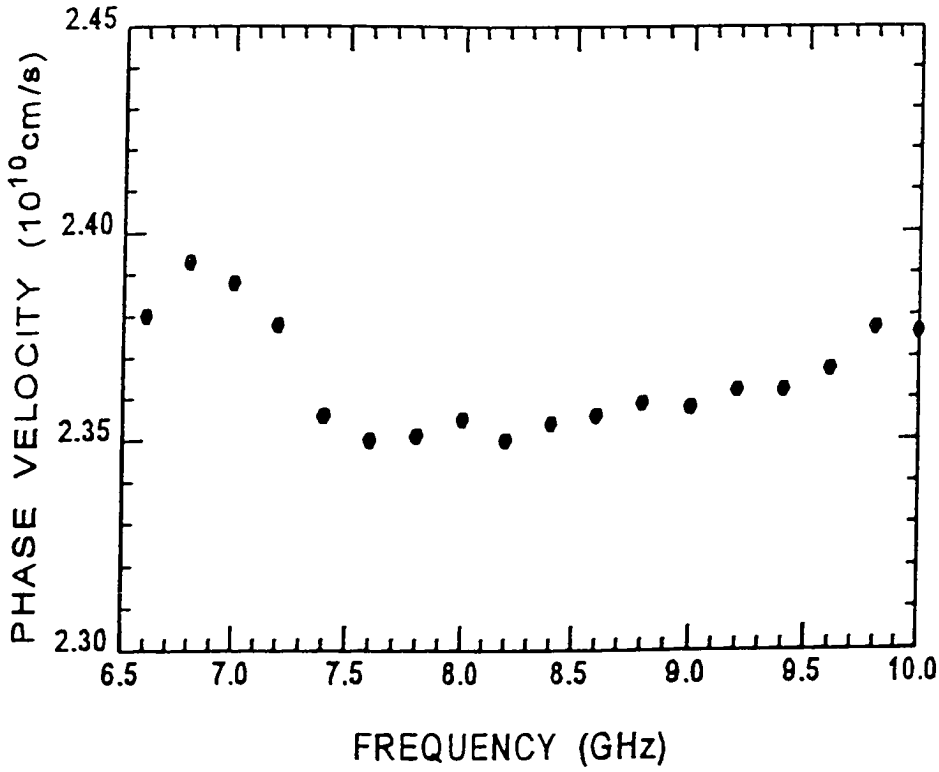

Fig. 30

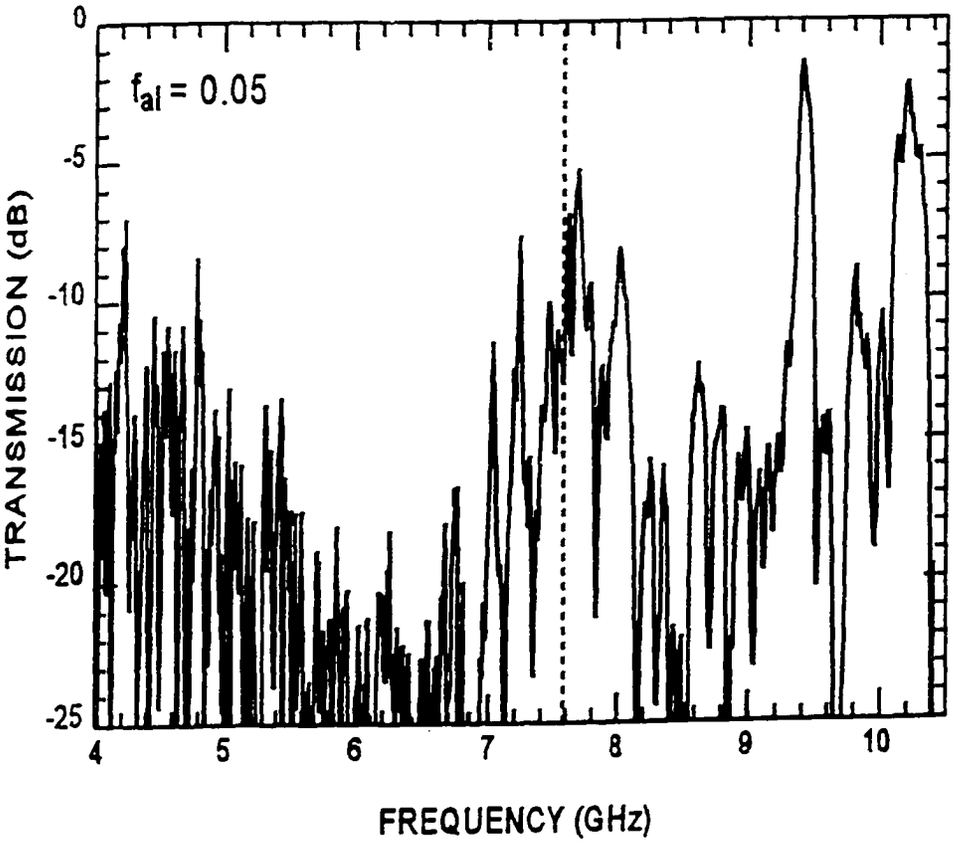

Fig. 31

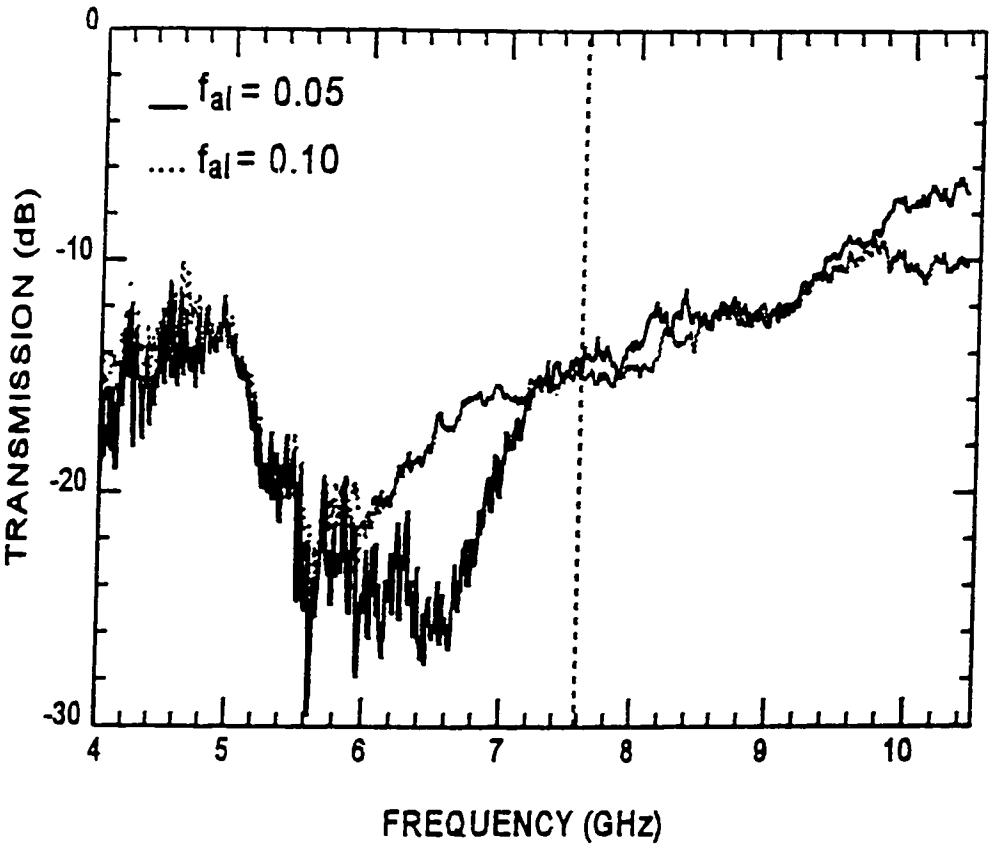

Fig. 32

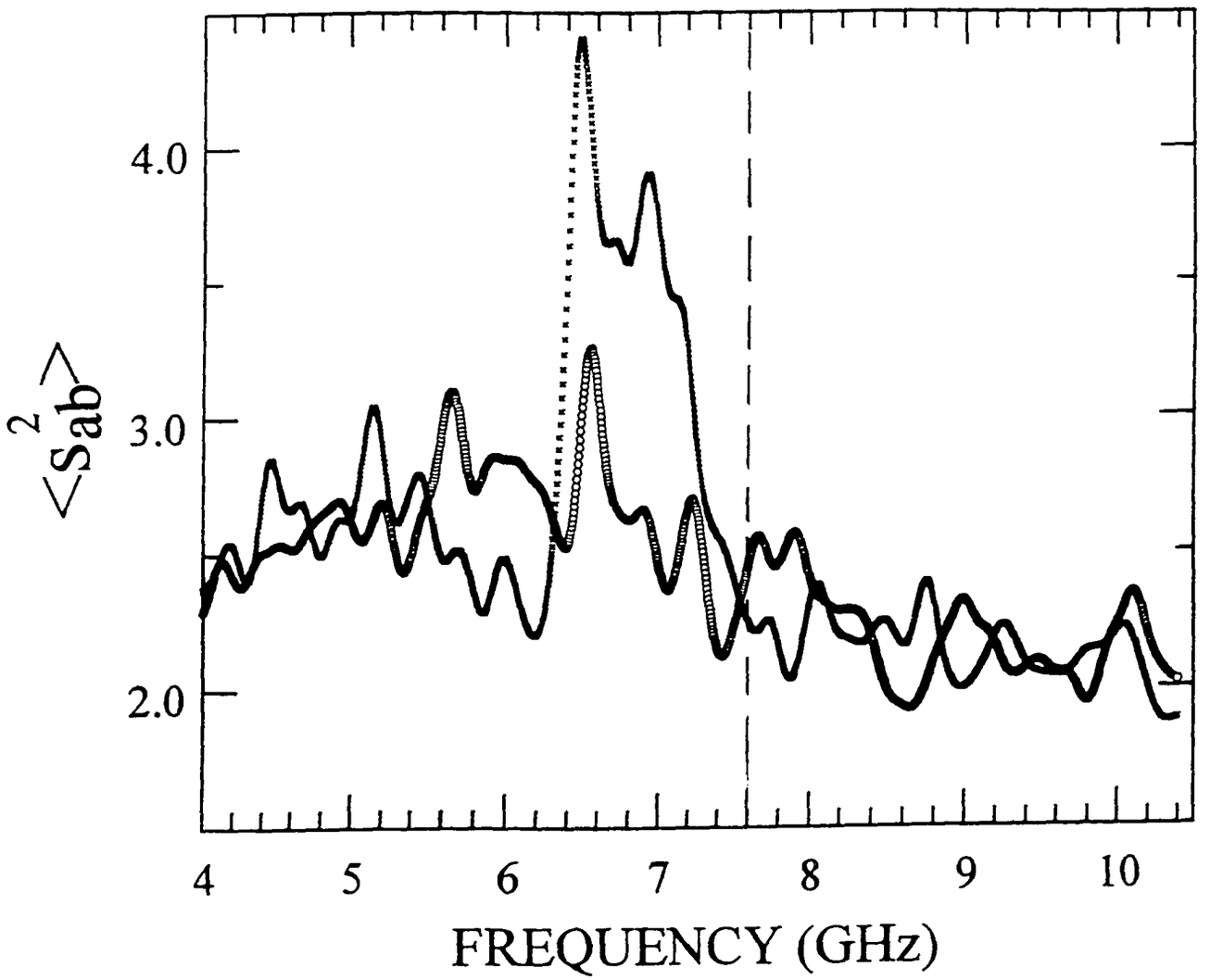

Fig. 33

REFERENCES

[1] For a comprehensive review on the problem see A. Ishimaru, *Wave Propagation and Scattering in Random Media* (Academic Press, Inc., London, 1978).

[2] Lord Rayleigh, Philos. Mag. **41**, 107 (1871).

[3] J. W. Goodman, *Statistical Optics* (J. Wiley, New York, 1985).

[4] B. Shapiro, Phys. Rev. B **34**, 4394 (1986).

[5] A. B. Fowler, A. Hartstein, and R. A. Webb, Phys. Rev. Lett. **48**, 196 (1982).

[6] C. P. Umbach, S. Washburn, R. B. Leibowitz and R. A. Webb, Phys. Rev. B **30**, 4048 (1984).

[7] B. L. Altshuler, Pis'ma Zh. Eksp. Teor. Fiz. **41**, 530 (1985) (JETP Lett. **41**, 648 (1985)).

[8] P. A. Lee and A. D. Stone, Phys. Rev. Lett. **55**, 1622 (1985).

[9] Y. Kuga and A. Ishimaru, J. Opt. Soc. Am. A **1**, 831 (1984); M. P. van Albada and A. Lagendijk, Phys. Rev. Lett. **55**, 2692 (1985); P. E. Wolf and G. Maret, Phys. Rev. Lett. **55**, 2696 (1985).

[10] E. Akkermans and R. Maynard, J. Phys. France Lett. **46**, L1045 (1985).

[11] B. Shapiro, Phys. Rev. Lett. **57**, 2168 (1986).

[12] A. Z. Genack, Phys. Rev. Lett. **58**, 2043 (1987).

[13] A. Z. Genack, Europhys. Lett. **11**, 331 (1990).

[14] G. Maret and P. E. Wolf, Z. Phys. B **65**, 409 (1987); M. Rosenblum, M. Hosen, I. Freund, and M. Kaveh, Phys. Rev. Lett. **58**, 2754 (1987); A. A. Golubentsev, Sov. Phys. JETP **59**, 26 (1984); M. J. Stephen, Phys. Rev. B **37**, 1 (1988); A. G. Yodh, P. D. Kaplan, and D. J. Pine, Phys. Rev. B **42**, 4744 (1990).

[15] For references to electronic correlation see *Mesoscopic Phenomena in Solids*, eds. B. L. Altshuler, P. A. Lee, and R. A. Webb (North-Holland, Amsterdam, 1991).

[16] M. J. Stephen and G. Cwilich, Phys. Rev. Lett. **59**, 285 (1987).

[17] P. A. Mello, Phys. Rev. Lett. **60**, 1089 (1988); P. A. Mello, E. Akkermans, and B. Shapiro, Phys. Rev. Lett. **61**, 459 (1988).

[18] B. Z. Spivak and A. Yu. Zyuzin, Solid State Comm. **65**, 311 (1988).

[19] S. Feng, C. Kane, P. A. Lee, and A. D. Stone, Phys. Rev. Lett. **61**, 834 (1988).

[20] R. Pnini and B. Shapiro, Phys. Lett. A **157**, 265 (1991); Phys. Rev. B **39**, 6986 (1989).

[21] E. Kogan and M. Kaveh, Phys. Rev. B **45**, 1049 (1992).

[22] N. Garcia and A. Z. Genack, Phys. Rev. Lett. **63**, 1678 (1989).

[23] A. Z. Genack, N. Garcia, and W. Polkosnik, Phys. Rev. Lett. **65**, 2129 (1990).

[24] M. P. van Albada, J. F. de Boer, and A. Lagendijk, Phys. Rev. Lett. **64**, 2787

(1990).

[25] J. F. de Boer, M. P. van Albada, and A. Lagendijk, Phys. Rev. B **45**, 658 (1992).

[26] S. John, Phys. Rev. Lett. **53**, 2169 (1984).

[27] J. B. Pendry and P. D. Kirkman, J. Phys. C **17**, 6711 (1984).

[28] P. W. Anderson, Philos. Mag. **52**, 505 (1985).

[29] P. Sheng and Z. Q. Zhang, Phys. Rev. Lett. **57**, 1879 (1986).

[30] C. A. Condat and T. R. Kirkpatrick, Phys. Rev. Lett. **58**, 226 (1987).

[31] N. Garcia and A. Z. Genack, Phys. Rev. Lett. **66**, 1850 (1991).

[32] A. Z. Genack and N. Garcia, Phys. Rev. Lett. **66**, 2064 (1991).

[33] E. Yablonovitch, Phys. Rev. Lett. **58**, 2059 (1987); S. John, Phys. Rev. Lett. **58**, 2486 (1987); E. Yablonovitch, T. J. Gmitter, and K. M. Leung, Phys. Rev. Lett. **67**, 2295 (1991); S. L. McCall, P. M. Platzman, R. Dalichaouch, D. Smith, and S. Schultz, Phys. Rev. Lett. **67**, 2017 (1991); J. Martorell and N. M. Lawandy, Phys. Rev. Lett. **65**, 1877 (1990).

[34] P. W. Anderson, Phys. Rev. **109**, 1492 (1958).

[35] M. Stoytchev and A. Z. Genack, Phys. Rev. B **55**, R8617 (1997).

[36] D. S. Wiersma, P. Bartolini, A. Lagendijk, and R. Righini, Nature **390**, 671 (1997).

[37] A. Chabanov and A. Z. Genack, unpublished

[38] A. F. Ioffe and A. R. Riegel, Prog. on Semi-conductors **4**, 237 (1960).

[39] D. J. Thouless, Phys. Rev. Lett. **39**, 1167 (1977).

[40] E. Abrahams, P. W. Anderson, D. C. Licciardello, and T. V. Ramakrishnan, Phys. Rev. Lett. **42**, 673 (1979).

[41] R. Landauer, Phil. Mag. **21**, 863 (1970).

[42] D. J. Thouless, Phys. Rep. **39C**, 93 (1974).

[43] M. Stoytchev and A. Z. Genack, Phys. Rev. Lett. **79**, 309 (1997).

[44] P. A. Mello, E. Akkermans, and B. Shapiro, Phys. Rev. Lett. **61**, 459 (1988).

[45] Th. M. Nieuwenhuizen and M. C. W. van Rossum, Phys. Rev. Lett. **74**, 2674 (1995).

[46] E. Kogan and M. Kaveh, Phys. Rev. B **52**, R3813 (1995).

[47] J. F. de Boer, M. C. W. van Rossum, M. P. van Albada, Th. M. Nieuwenhuizen, and A. Lagendijk, Phys. Rev. Lett. **73**, 2567 (1994).

[48] M. Stoytchev and A. Z. Genack, submitted to Phys. Rev. Lett.

[49] S. John, Phys. Rev. Lett. **58**, 2486 (1987).

[50] For a review, see: *Development and Applications of Materials Exhibiting Photonic Band Gaps*, special issue of J. Opt. Soc. Am. B **10**, 208 (1993); *Photonic*

Band Gaps and Localization, ed. C. M. Soukoulis (Plenum Press, New York, 1993).

[51] K. M. Ho, C. T. Chan, and C. M. Soukoulis, Phys. Rev. Lett. **65**, 3152 (1990).

[52] C. T. Chan, K. M. Ho, and C. M. Soukoulis, Europhys. Lett. **110**, 563 (1991).

[53] J. B. Pendry and A. MacKinnon, Phys. Rev. Lett. **69**, 2772 (1992).

[54] A. R. McGrun and A. A. Maradudin, Phys. Rev. B **48**, 17576 (1993).

[55] D. R. Smith, S. Shultz, N. Kroll, M. Sigalas, K. M. Ho, and C. M. Soukoulis. Appl. Phys. Lett. **65**, 645 (1994).

[56] M. Sigalas, C. T. Chan, K. M. Ho, and C. M. Soukoulis, Phys. Rev. B **52**, 11744 (1995).

[57] E. Yablonovitch, T. J. Gmitter, and K. M. Leung, Phys. Rev. Lett. **67**, 2295 (1991).

[58] E. Yablonovitch, T. J. Gmitter, R. D. Meade, A. M. Rappe, K. D. Brommer, and J. D. Joannnopoulis, Phys. Rev. Lett. **67**, 3380 (1991).

[59] E. Ozbay, A. Abeyta, G. Tuttle, M. Tringides, R. Biswas, C. T. Chan, C. M. Soukoulis, and K. M. Ho, Phys. Rev. B **50**, 1945 (1994).

[60] D. Sievenpiper, M. Sickmiller, and E. Yablonovitch, Phys.Rev. Lett. **76**, 2480 (1996).

[61] A. D. Stone, P. A. Mello, K. A. Muttalib, and J. L. Pichard, *Mesoscopic Phe-*

nomena in Solids, eds. B. L. Altshuler, P. A. Lee, and R. A. Webb (Elsevier, 1991).

[62] N. Garcia, A. Z. Genack, R. Pnini, and B. Shapiro, Phys. Lett. A **176**, 458 (1993).

[63] R. Pnini and B. Shapiro, private communication.

[64] N. Shnerb and M. Kaveh, Phys. Rev. B **43**, 1279 (1991).

[65] A. Z. Genack and N. Garcia, Europhys. Lett. **21**, 753 (1993).

[66] M. C. W. van Rossum, Ph. D. Thesis.

[67] C. W. J. Beenakker, Rev. Mod. Phys. (1997).

[68] Th. Martin and R. Landauer, Phys. Rev. B **45**, 1742 (1992).

[69] Y. Imry, Europhys. Lett. **1**, 249 (1986).

[70] O. N. Dorokhov, Solid State Comm. **51**, 381 (1984).

[71] *The scattering and localization of classical waves*, edited by P. Sheng (World Scientific, Singapore, 1990).

[72] *Mesoscopic phenomena in solids*, edited by B. L. Altshuler, P. A. Lee, and R. A. Webb (North-Holland, Amsterdam, 1991).

[73] S. A. van Langen, P. W. Brouwer, and C. W. J. Beenakker, Phys. Rev. E **53**, 1344 (1996).

[74] A. Z. Genack, N. Garcia, and A. A. Lisyansky, in *Photonic band gaps and localization*, edited by C. M. Soukoulis (Plenum Press, New York, 1993).

[75] M. Stoytchev and A. Z. Genack, in preparation.

[76] J. C. Dainty, *Laser Speckle and Related Phenomena, Topics in Applied Physics v. 9*, ed. J. C. Dainty (Springer-Verlag, Berlin, 1984).

[77] R. L. Weaver, Phys. Rev. B **47**, 1077 (1993).

[78] M. Yosefin, Europhys. Lett. **25**, 675 (1994).

[79] P. W. Brouwer, (Cond-matt/9711113) to be published.

[80] E. Kogan, M. Kaveh, R. Baumgartner, and R. Berkovits, Phys. Rev. B **48**, 9404 (1993).

[81] A. Lagendijk, R. Vreeker, and P. de Vries, Phys. Lett. A, **136**, 81 (1989).

[82] P. Pradhan and N. Kumar, Phys. Rev. B **50**, 9644 (1994).

[83] J. C. J. Paasschens, T. Sh. Misirpashaev and C. W. J. Beenakker, Phys. Rev. B **54**, 11887 (1996).

[84] P. W. Brouwer, private communication.

[85] M. C. W. van Rossum and Th. M. Nieuwenhuizen, Phys. Lett. A **177**. 452 (1993).

[86] M. C. W. van Rossum and Th. M. Nieuwenhuizen, submitted for publication.

[87] M. C. W. van Rossum, Th. M. Nieuwenhuizen, and R. Vlaming, Phys. Rev. E **51**, 6158 (1995).

[88] N. F. Mott and E. A. Davis, *Electronic Processes in Non-crystalline Materials*, 2nd ed. (Oxford University Press, New York, 1979).

[89] I. M. Lifshitz, Nuovo Cim. (Suppl. 1) 3, 591 (1956), I. M. Lifshitz and A. M. Kosevich, in: *Lattice Dynamics* (Benjamin, New York, 1969), p. 53

[90] A. A. Maradudin, E. W. Montroll, G. H. Weiss, and I. P. Ipatova, *Theory of Lattice Dynamics in the Harmonic Approximation*, 2nd ed. (Academic Press, New York, 1971), Ch. VIII.

[91] J. D. Joannopolos, R. D. Meade, and J. N. Winn, *Photonic Crystals* (Princeton University Press, Princeton, 1995), Ch. VI.

[92] J. D. Jackson, *Classical Electrodynamics*, (John Wiley & Sons, New York, 1990), Ch. VIII.

[93] D. E. Aspnes, Am. J. Phys. **50**, 704 (1982).

IMAGE EVALUATION TEST TARGET (QA-3)

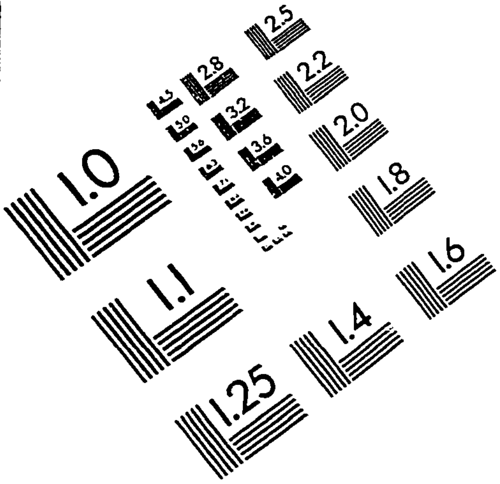

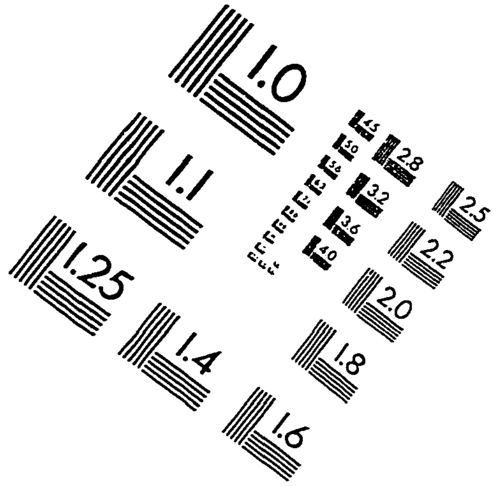

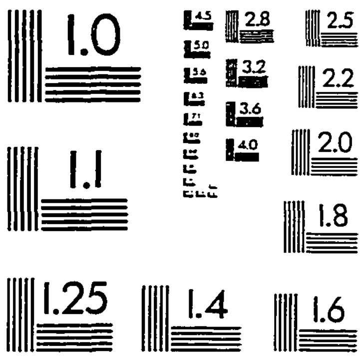

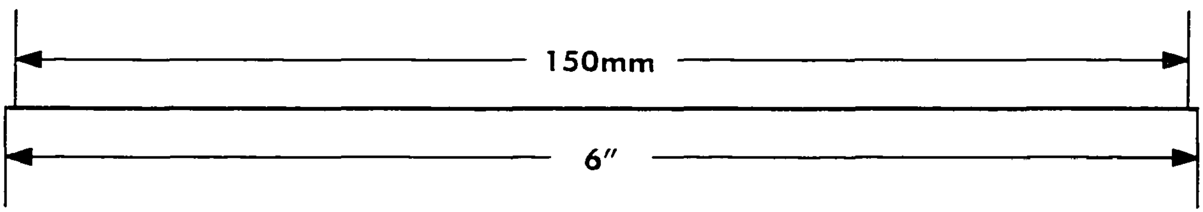

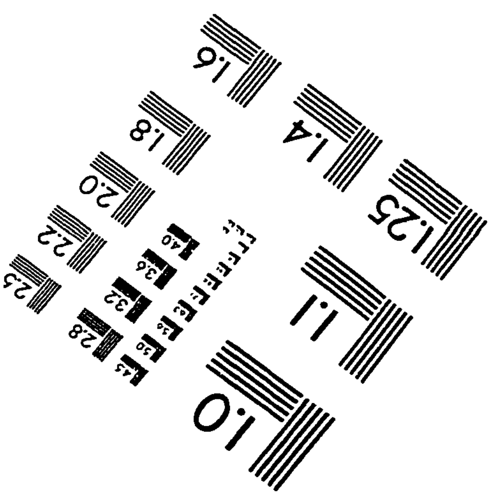

APPLIED IMAGE . Inc
1653 East Main Street
Rochester, NY 14609 USA
Phone: 716/482-0300
Fax: 716/288-5989